



Respiratory complex I regulates dendritic cell maturation in explant model of human tumor immune microenvironment

Rita Turpin,¹ Ruixian Liu,¹ Pauliina M Munne,¹ Aino Peura,¹ Jenna H Rannikko,² Gino Philips,³ Bram Boeckx,⁴ Natasha Salmelin,¹ Elina Hurskainen,¹ Iida Suleymanova,¹ July Aung,⁵ Elisa M Vuorinen,⁶ Laura Lehtinen,⁶ Minna Mutka,⁷ Panu E Kovanen,⁸ Laura Niinikoski,⁹ Tuomo J Meretoja,⁹ Johanna Mattson,¹⁰ Satu Mustjoki ^{11,12} Päivi Saavalainen,⁶ Andrei Goga,¹³ Diether Lambrechts,¹⁴ Jeroen Pouwels,¹ Maija Hollmén,² Juha Klefström ^{1,15}

To cite: Turpin R, Liu R, Munne PM, *et al.* Respiratory complex I regulates dendritic cell maturation in explant model of human tumor immune microenvironment. *Journal for ImmunoTherapy of Cancer* 2024;**12**:e008053. doi:10.1136/jitc-2023-008053

► Additional supplemental material is published online only. To view, please visit the journal online (<https://doi.org/10.1136/jitc-2023-008053>).

RL and PMM contributed equally.

Accepted 04 March 2024



© Author(s) (or their employer(s)) 2024. Re-use permitted under CC BY-NC. No commercial re-use. See rights and permissions. Published by BMJ.

For numbered affiliations see end of article.

Correspondence to

Dr Juha Klefström;
juha.klefstrom@helsinki.fi

ABSTRACT

Background Combining cytotoxic chemotherapy or novel anticancer drugs with T-cell modulators holds great promise in treating advanced cancers. However, the response varies depending on the tumor immune microenvironment (TIME). Therefore, there is a clear need for pharmacologically tractable models of the TIME to dissect its influence on mono- and combination treatment response at the individual level.

Methods Here we establish a patient-derived explant culture (PDEC) model of breast cancer, which retains the immune contexture of the primary tumor, recapitulating cytokine profiles and CD8+T cell cytotoxic activity.

Results We explored the immunomodulatory action of a synthetic lethal BCL2 inhibitor venetoclax+metformin drug combination *ex vivo*, discovering metformin cannot overcome the lymphocyte-depleting action of venetoclax. Instead, metformin promotes dendritic cell maturation through inhibition of mitochondrial complex I, increasing their capacity to co-stimulate CD4+T cells and thus facilitating antitumor immunity.

Conclusions Our results establish PDECs as a feasible model to identify immunomodulatory functions of anticancer drugs in the context of patient-specific TIME.

INTRODUCTION

While a common denominator of cancer is a dysregulation of the tumor immune microenvironment (TIME), the actual composition and function of the TIME is both tumor type-specific and patient-specific.¹ Characterizing the TIME is improving the stratification of patients who may respond to immunomodulatory monotherapies, like anti-CTLA-4 or anti-programmed cell death 1 (PD-1)/programmed death ligand 1 (PD-L1).² However, it is increasingly clear that the TIME also has a strong role in influencing the outcome of cytotoxic chemo-

WHAT IS ALREADY KNOWN ON THIS TOPIC

⇒ Clinical studies in breast cancer indicate the limited efficacy of immune checkpoint inhibitors alone, emphasizing the importance of simultaneously targeting tumor cells and immune cells. The study delves into the complexity of tumor immune microenvironment dynamics and the need for a comprehensive understanding to optimize combination immunotherapies for personalized treatment.

WHAT THIS STUDY ADDS

⇒ This work showcases the patient-derived explant culture (PDEC) model's efficacy for mechanistic studies drug effects on the tumor immune microenvironment. The PDEC model retains the immune composition of primary breast tumors, and these resident immune cells may be activated to evaluate the antitumor response of compounds. Importantly, we can simultaneously quantify cell death of tumor cells and immune cell subtypes, possibly predicting drug-induced lymphopenia. The study reveals metformin's capacity to induce dendritic cell (DC) maturation, subsequently prompting CD4+T cell proliferation.

HOW THIS STUDY MIGHT AFFECT RESEARCH, PRACTICE OR POLICY

⇒ By revealing the role of metformin in promoting DC maturation through Complex I inhibition, the study suggests a potential strategy to enhance immunotherapy treatments. This insight could influence the development of combination therapies that leverage the immunomodulatory effects of metformin to improve treatment outcomes.

targeted therapies which were not meant to, or do not affect immune cells directly. While the release of tumor antigens by tumor toxic compounds could trigger a beneficial

immune response,^{3,4} the drug toxicity also targets mitotically active immune cells with potentially negative effects on antitumor immune responses.^{5,6} Furthermore, chemo-induced immunogenic cell death can, in certain circumstances, act as a trigger for the recruitment of pro-tumor macrophages,⁷ which can reduce the sensitivity of cancer cells to paclitaxel, etoposide, and doxorubicin.⁸

Recent clinical studies in breast cancer (BC) have also shown that targeting the immune system through the PD-1/PD-L1 pathway alone is not effective,^{9–11} whereas a combination of paclitaxel+anti-PD-L1, designed to target the tumor and the TIME simultaneously, has provided clinical evidence of efficiency to support approval.^{12,13} In fact, the concept of targeting tumor cells and immune cells simultaneously is so widely tested as a treatment modality for different cancer types that nearly 90% of current PD-1/PD-L1-targeted trials include a combination therapy.¹⁴

These notions highlight that defining anticancer drug effects on not only tumor cells, but also on the TIME is crucial to understand how the drug's action translates into efficacy in the context of a heterogeneous tumor microenvironment. A better understanding of which immune cell types are activated, depleted, or otherwise impacted under the treatment, would provide important clinical trajectories, especially for a choice of the right combination of immunotherapies in a personalized treatment setting.^{15,16} Synthetic lethality (SL) is a concept that describes the selective killing of cancer cells that harbor specific alterations of an oncogenic or tumor suppressor pathway, with a drug that is toxic to cancer cells due to specific drug-sensitizing mutations, but is much less toxic to normal cells that are lacking the mutations.¹⁷ The MYC gene is amplified, or the MYC-encoded protein is elevated through other mechanisms, in up to 70% of human cancers.¹⁸ The elevated or deregulated MYC levels drive many oncogenic processes, including metabolic reprogramming and non-stop cell cycle progression, but MYC also sensitizes cells to diverse inducers of extrinsic or intrinsic programmed cell death pathways.^{19–22} These early findings have laid the conceptual foundation for MYC-dependent SL (MYC SL) therapeutic strategies, which seek to specifically harness MYC-generated vulnerability pathways as opposed to drugging the MYC protein directly.^{23–25} A previous study exploring therapeutic opportunities through the MYC SL concept revealed that in several mouse models of MYC high BC, the MYC-high tumors *in vivo* are specifically vulnerable to combination treatment with venetoclax and metformin. Venetoclax is a BH3-mimetic that blocks the anti-apoptotic B-cell lymphoma-2 (BCL-2) protein²⁶ and metformin is a commonly prescribed drug for type 2 diabetes.²⁷ In particular, the treatment of syngrafted Wap-Myc tumors in mice with the venetoclax+metformin (VeM) combination results in cessation of tumor growth and the addition of anti-PD-1 checkpoint inhibitor to the treatment regimen results in a persistent treatment response—with no tumors growing in the mice even after drug withdrawal. While these

observations are consistent with the idea of immunogenic cell death as a mechanism of VeM *in vivo*, emerging evidence also suggests an important immunomodulatory function for metformin; it can maintain high cytotoxic T lymphocyte (CTL) activity in tumor cells²⁸ through enhancing the anti-apoptotic abilities of CD8+T cells and downmodulating PD-1/PD-L1.^{29,30} Therefore, the anti-cancer effects observed with the VeM combination raises the interesting question whether metformin only acts by boosting cancer cell death, or whether it somehow modulates an immune response directly.

We previously developed a method to grow three-dimensional (3D) cultures of intact fragments of primary human patient-derived breast and BC tissue. The patient-derived explant culture (PDEC) model offers many advantages over conventional reductionist and artifact-prone cell co-culture and rodent models, and it has provided new insights into the biology of BC subtypes, as well as mechanisms of treatment regimens in the context of authentic human breast tumor tissue.^{27,31–33} Since PDECs come directly from surgery, they contain viable immune cells. We considered that PDECs could offer a unique method to simultaneously investigate the effects of VeM on tumor cells and tumor resident immune cells in *ex vivo* conditions.

Here, we first show that PDECs maintain the immune composition and baseline immune activity of the primary breast tumors. In addition, we demonstrate that the cytolytic activity of PDEC-containing T cells can be activated with a direct T-cell activator, anti-CD3/CD28/CD2, but not via the PD-1/PD-L1 mechanism. Venetoclax depleted tumor-infiltrating lymphocytes in PDECs, as previously observed in mice,³⁴ an effect that was not counteracted by metformin. However, we report that metformin surprisingly promotes human dendritic cell (DC) maturation by altering the immune cell metabolism through the inhibition of respiratory complex I (CI). The metformin-induced DC maturation can trigger CD4+T cell proliferation, suggesting the inhibition of CI or other sites of mitochondrial respiration as a potential new therapeutic strategy to enhance immunotherapy.

RESULTS

PDECs maintain the immune contexture and baseline immune activity of the primary breast tumor

To define whether PDECs preserve components of the primary TIME, we investigated the presence of CD45+leukocytes in the tumor explant cultures using confocal immunofluorescence microscopy. The analysis of explants from five different patients after 3 days of *ex vivo* culture showed the presence of CD45+leukocytes in all studied cultures (figure 1A). To determine how well PDECs recapitulate the immune cell composition of the primary tumor sample, a workflow was designed to compare the general composition of tumor-infiltrating leukocytes (TILs) of primary tumors, with their corresponding PDECs up to 1 week in culture (figure 1B). First,

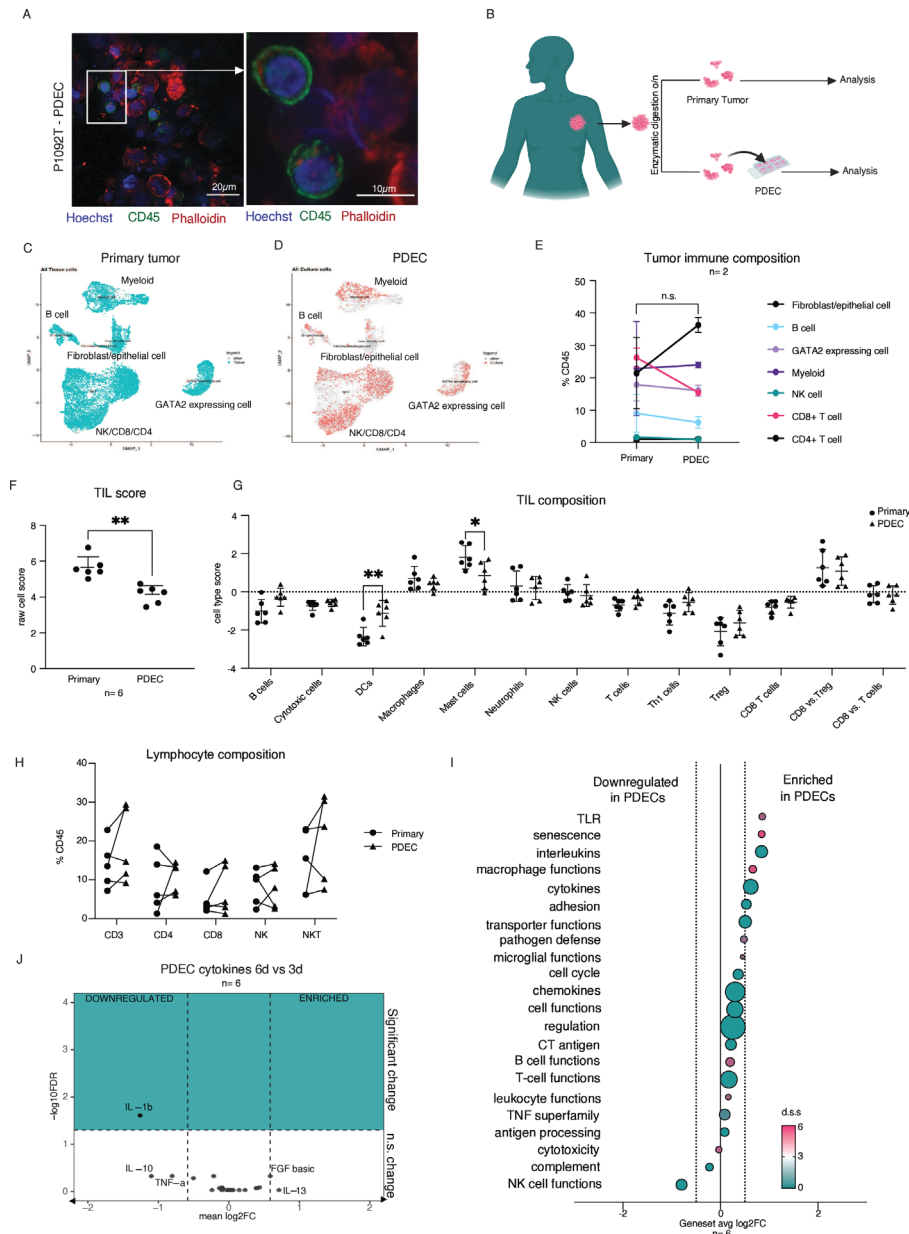


Figure 1 PDECs maintain the immune contexture and baseline immune activity of primary breast tumor. (A) Immunofluorescent staining of CD45 and F-actin in PDECs after 72 hours in culture. P1092T refers to a tumor sample from patient 1092. (B) Schematic representation of workflow comparing primary tumor tissue to cultured tumor tissue (PDEC). (C) Single-cell RNA sequencing UMAPs after data integration from n=2 primary tumors, (D) and the corresponding PDECs. (E) Immune cell composition of primary tumors compared with the two corresponding PDECs. No significant changes were detected between any immune subtypes using the MASC algorithm (F) gene expression profiling of leukocytes of biologically independent primary tumors and their corresponding PDECs shows a decrease in TIL gene expression ($p=0.0013$) after 72 hours in culture ($n=6$). Statistics were done with paired t-test with two-tailed p value. (G) Immune cell composition obtained from gene expression profiling of samples from (F) normalized to nSolver tumor infiltrating leukocyte gene signature. Dendritic cell ($p=0.0032$) and mast cell ($p=0.0481$) numbers were significantly affected in culture. Statistics are two-way analysis of variance with Sidaks multiple comparison test. (H) Flow cytometry analysis of CD3+T cells, CD4+T helper cells, CD8+T effector cells, NK, and NKT cells from primary tumors and corresponding PDECs ($n=8$) with no significant differences between primary tumor and PDECs (I) estimation of immune cell activity pathways from NanoString gene expression profiling normalized to TIL numbers. The pink fuchsia color indicates directional significance (t-statistic for each gene against each covariate) pathways considered significantly different are those with an average log2fold change of >0.5 in addition to statistically significant overexpression as determined by the directional significance score above 0. (J) Cytokine profiling of explant media at 72 hours, and 144 hours. Cytokines below -0.58 log2FC are downregulated more than 1.5-fold, and those with $-\log_{10}FDR$ of 1.3 or greater are significant. Cytokine statistics were computed with one-sample t-test for deviance from 0. P values were adjusted by the FDR method. All data are presented as mean values \pm SD. FDR, false discovery rate; IL, interleukin; NK, natural killer; NKT, natural killer T; PDEC, patient-derived explant culture; TIL, tumor-infiltrating leukocytes; TLR, toll-like receptor; TNF, tumor necrosis factor

the immune cell composition of two donors was analyzed using single-cell RNA sequencing of sorted CD45+leukocytes comparing primary tumor material to explants grown for 1 week. The results demonstrated that myeloid cells, B cells, NK (natural killer) cells, CD8+T cells, and CD4+T cells were preserved in PDECs in similar proportions as the primary tumor, with no significant differences between cell types (figure 1C–E; online supplemental figure 1A,B). Second, while NanoString nSolver Gene expression profiling at 3 days in culture revealed an overall decrease in TILs within explants (figure 1F), the composition of the TILs which includes B cells, cytotoxic cells, macrophages, neutrophils, NK cells, T cells (including Th1, regulatory T cells (Treg), and CD8+) was surprisingly similar (figure 1G). We did, however, observe a decrease in the proportion of mast cells, and an increase in the proportion of DCs (figure 1G). Third, a flow cytometric comparison of CD45+leukocytes of the primary tumors and PDECs cultured ex vivo for 1 week confirmed that the relative numbers of lymphocytes (CD4+ and CD8+ T cells, NK, Natural Killer T (NKT) cells) were not significantly altered (figure 1H).

To determine the baseline activity status of primary tumor versus PDEC TILs, the gene expression profiling samples were processed to remove systematic differences in TIL numbers, and further analyzed for cell and immune activity gene sets (figure 1I). The basal activity of pathways including NK cell functions, T-cell functions, B-cell functions, cytokines and interleukins was similar to the primary tumor sample (online supplemental figure 1C). Only a few pathways, including toll-like receptor (TLR), senescence, and macrophage functions, were significantly different but we note that their corresponding profiles consisted of a small number of genes (online supplemental figure 1D). Additionally, longitudinal cytokine profiling up to 1-week revealed a significant decrease in only one cytokine, IL-1b, while the other 26 were not significantly changed (figure 1J). These results suggest that the PDEC cultures themselves have little effect on the baseline activity of the immune cells. Overall, these results indicate that the PDEC model preserves the TIME of the primary patient tumor during a 7-day culture period.

Resident tumor-infiltrating T cells can be activated to kill tumor cells ex vivo

The presence of CD45+cells, including cytolytic cells of both innate (NK, NKT) and acquired immunity (CD8+T cells), led us to ask whether these cells could be functionally activated. We used a commercially available soluble antibody complex, anti-CD3/CD28/CD2, which cross-links the surface ligands CD2, CD3, and CD28 on T cells to provide stimulatory and co-stimulatory signals needed for robust T-cell activation, herein referred to as anti-CD3/CD28/CD2. We compared anti-CD3/CD28/CD2 to therapeutically relevant antibodies for PD-1 and its ligand (PD-L1) (programmed death ligand 1) to detect the “maximum” T-cell response in PDECs, and to determine

whether in our PDEC model the PD-1-PD-L1-axis is a critical signaling pathway that limits the physiological activity of resident T cells.³⁵

We treated the explants for 72 hours and measured general cell death with the CellTox green assay, observing a statistically significant increase in cell death on anti-CD3/CD28/CD2 treatment whereas no cell death was observed following treatment with anti-PD-L1 (figure 2A,B). We randomly chose three primary tumor samples from the CellTox experiment and performed multiplex immunohistochemistry (IHC) to confirm that the samples contained immune cells, and that the cell death was a result of T-cell cytotoxicity (figure 2C; online supplemental figure 2A). To further verify that any cell death seen following anti-CD3/CD28/CD2 likely came from tumor cells, we performed flow cytometric analysis of PDECs, and quantified absolute numbers of CD45–non-hematopoietic cell populations, which were mostly tumor cells, but also stromal cells like fibroblasts. Here we also observed a reduction of tumor cells after T-cell activation (figure 2D). We further stained and imaged multiple fragments within PDEC cultures of the same patient and found that immune cells are retained in the intratumoral regions evenly throughout the culture, decreasing the chance that any response is due largely due to uneven distribution of immune cells between wells (online supplemental figure 2B,C,D).

Consistent with an increase in cytotoxic activity leading to cell death, quantitative polymerase chain reaction (qPCR) analysis of PDECs following anti-CD3/CD28/CD2 treatment revealed a statistically significant increase in interferon (IFN)- γ expression, and a trend for elevated messenger RNA (mRNA) expression of granzyme B (GZMB) and perforin-1 (PRF1) (figure 2E–H). Both PRF1 and GZMB are expressed by cytotoxic T cells and NK cells on activation, while IFN- γ is a signature proinflammatory cytokine typically used to measure immune activation.^{36–37} The cell death and mRNA results in response to anti-CD3/CD28/CD2, along with the fact that anti-PD-L1 monotherapy has no positive effect on tumor cell death, or the transcription of *IFN- γ* , *GZMB*, or *PRF1*, reinforce the idea that the cell death seen previously is likely a result of T cell receptor (TCR)-triggering, and the downstream effects of T-cell activation.

We profiled cytokines of T-cell activation and inflammation from PDEC supernatant after 72 hours of anti-CD3/CD28/CD2 (n=16), and anti-PD-L1 (n=6) treatments. The results highlight the ability of PDECs to reflect patient heterogeneity, while still capturing the general trend of cytokines expected after robust T-cell activation (figure 2I,J). For example, we observed an increase in interleukin (IL)-2 which is secreted by CD4+T cells on antigen stimulation, and in IL-10, which is secreted in response to immune activation by several different cell types^{38–39} (figure 2I). In accordance with the previous qPCR findings, we observed that unlike anti-CD3/CD28/CD2 treatment, anti-PD-L1 monotherapy did not deviate far from the control, suggesting negligible effect from the

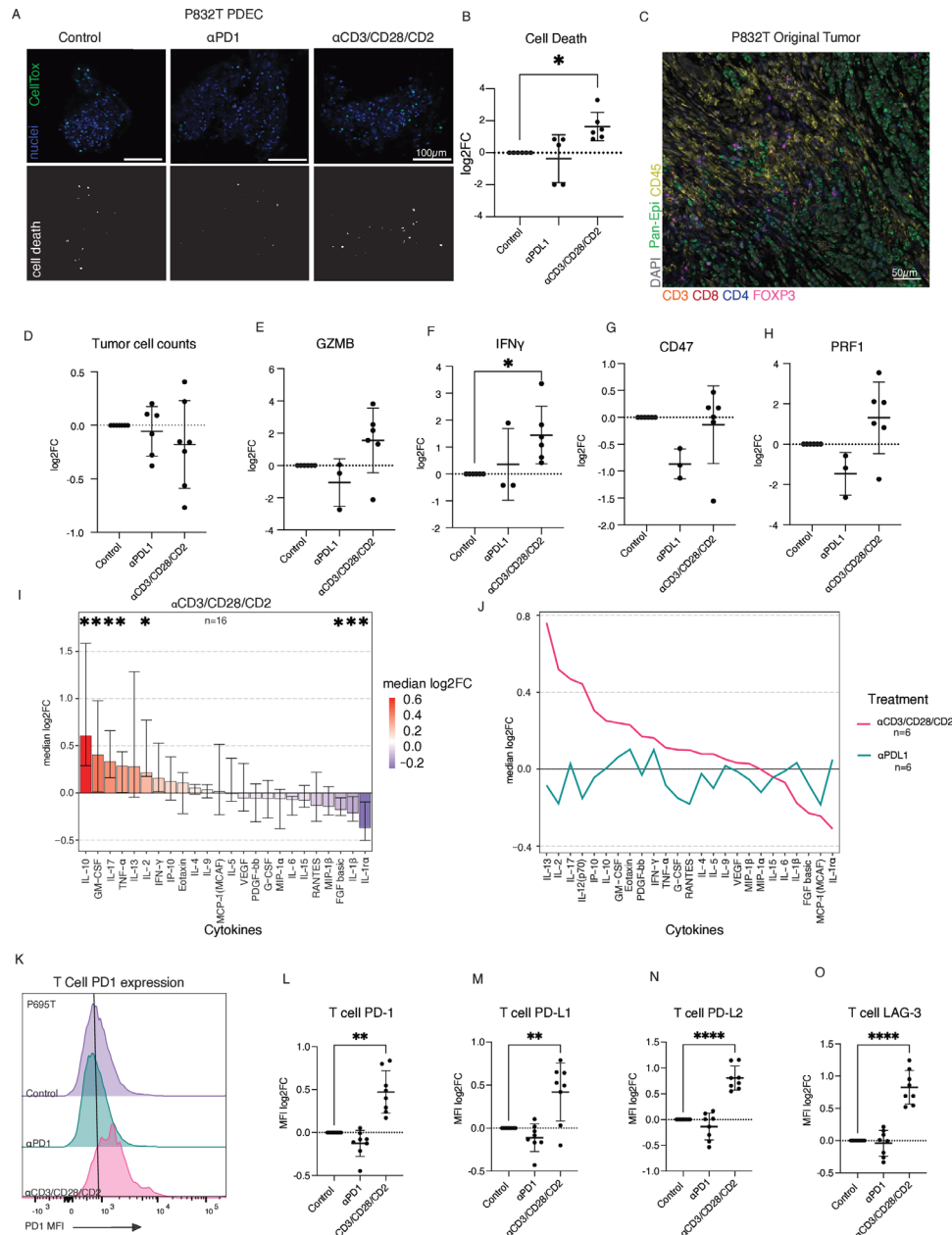


Figure 2 Resident tumor-infiltrating T cells can be activated to kill tumor cells ex vivo. (A) CellTox staining of P832T PDEC following treatment with a-PD-1 and anti-CD3/CD28/CD2. (B) Quantification of cell death from IF images corresponding to $n=6$ biologically independent PDECs, showing significant cell death following anti-CD3/CD28/CD2 treatment ($p=0.0321$) quantified with a one-way ANOVA with Fisher's exact test. (C) Immune infiltration of primary tumor from which PDECs in figure 3A. were derived from. (D) Tumor cell (CD45 $-$) counts in $n=7$ biologically independent PDECs ($n=6$ for aPD-L1) following aPD-L1 and antiCD3/CD28/CD2 treatment as the \log_2FC of the absolute cell numbers normalized the control (E–H) qPCR analysis of *GZMB*, *IFN- γ* ($p=0.0208$), *CD47*, *PRF1* relative to the control. $n=3$ for aPD-L1, $n=6$ for control and anti-CD3/CD28/CD2-treated. Statistical significance was tested with a one-way ANOVA with Fisher's exact test. Data are presented as mean values \pm SD. (I) Multiplex cytokine profiling of PDECs after 72 hours anti-CD3/CD28/CD2 treatment $n=16$. Each cytokine is tested with a one-sample non-parametric Wilcoxon test for deviance from 0 (no change) and p values adjusted by an FDR method. Cytokines are ordered by median \log_2FC and plotted with error bars ranging the IQR. (J) Comparison of median \log_2FC of cytokines between anti-CD3/CD28/CD2 and aPD-L1 treatments in PDECs $n=6$. (K) Flow cytometry representation of median fluorescence intensity of checkpoint marker, PD-1, on CD3+T cells in control, aPD-1 and anti-CD3/CD28/CD2-treated PDEC of P695T. (L–O) Graphs quantifying the median surface expression of T-cell checkpoint proteins relative to control. Statistical significance was tested with significant increase in PD-1 ($p=0.0010$), PD-L1 ($p=0.0096$), PD-L2 ($p<0.0001$), and LAG-3 ($p<0.0001$) in response to anti-CD3/CD28/CD2. Statistical significance was tested with a one-way ANOVA with Fisher's exact test. Data are presented as mean values \pm SD. ANOVA, analysis of variance; aPD-1, anti-programmed cell death 1; aPD-L1, anti-programmed death ligand 1; FDR, false discovery rate; *GZMB*, granzyme B; IF, immunofluorescence; IFN, interferon; LAG-3, lymphocyte activation gene 3; MFI, median fluorescence intensity; PD-1, programmed cell death 1; PDEC, patient-derived explant culture; PRF1, perforin-1; PD-L1, programmed death ligand 1; PD-L2, programmed death ligand 2; qPCR, quantitative polymerase chain reaction.

drug in terms of induced cytokine expression (figure 2J). For T cell-specific analysis, CD3+T cells were profiled directly for signs of exhaustion following treatment by flow cytometry, measuring the median fluorescent intensity of checkpoint ligands/receptors programmed death ligand 2 (PD-L2), PD-L1, lymphocyte-activation gene 3 (LAG3), and PD-1 on the surface of the cells. Once again, anti-CD3/CD28/CD2, but not anti-PD-1, induced expression of these checkpoint molecules, suggestive of T-cell activation (figure 2K–O; online supplemental figure 2E). The transcriptional and cytokine data support the general detection of immune activation within PDEC cultures, while Immunofluorescence (IF) and flow cytometry analysis of PDECs suggest that T cells are functionally activatable to kill tumor cells ex vivo.

Together, the presence of the primary tumor TIL repertoire within PDECs and the evidence for activatable cytolytic properties in the tumor CD8+T cells demonstrate PDECs as a versatile model to study various aspects of tumor-immune tissue interactions and anticancer drug responses in the context of the TIME.

Assessment of combination therapy with venetoclax reveals lymphodepletion of T cells

Since the PDECs preserved the TIME, we recognized an opportunity to further explore and validate the specific responses of tumor cells and TIME to the VeM combination, which shows strong in vivo antitumor activity in several mouse models of MYC-driven aggressive BC.²⁷ Clinically, venetoclax has been observed as a lymphodepleting agent as it induces apoptosis in BCL-2 reliant subsets of T cells.³⁴ The lymphodepleting activity is a potential clinical concern, as it could negatively impact immune system functions and reduce the opportunities to combine venetoclax with immune-modulating therapies. We first tested the idea that metformin component of VeM perhaps affords protection to immune cells against the lymphodepleting actions of venetoclax, which could explain the better in vivo effect of VeM in comparison to single treatments.²⁷ In parallel with VeM, we treated PDECs with clinically relevant paclitaxel, a chemotherapy used to treat primary breast tumors, often in combination with other drugs (figure 3A).

Unsupervised clustering of cytokines of 10 patient samples revealed tight clustering by treatment. We observed a consistent downregulation of most T-cell-associated cytokines (as determined in figure 2I) in response to VeM, irrespective of MYC-status, suggestive of a depletion of lymphocytes (figure 3B, online supplemental figure 3A). Flow cytometry analysis of CD45-cells, mainly tumor cells, showed some variation in the level of apoptotic responses to VeM between independent PDEC samples (figure 3C,D), whereas every VeM-treated sample showed a noticeable drop in the number of CD4+ and CD8+ T cells, with a more significant decrease in the numbers of CD8+T cells (figure 3E,F). Although we failed to see tumor cytotoxicity in PDECs after paclitaxel treatment, likely due to a delay between the drug's

primary and secondary modes of action ex vivo,⁴⁰ we did notice an increase in inflammatory cytokines suggestive of inflammation (IL-2, IL-10, IL-4, IL-15) from a subset of patients. We took a transcriptional approach to broaden the variety of immune cell types we could observe simultaneously (figure 3G). As with the cytokine profiling and flow cytometry, we noticed a clear diminishing impact of VeM on T cells. These results led us to refute the initial working hypothesis suggesting that metformin protects BCL-2-reliant CTLs against the lymphodepleting effects of venetoclax since none of our experiments supported this notion.

Metformin contributes to dendritic cell activation ex vivo and in vivo

The fact that metformin did not protect T cells from apoptosis following venetoclax treatment led us to hypothesize that the immunogenic benefits of metformin might derive from the immune cells that were spared within the PDEC tumor microenvironment; for example, DCs, macrophages, and NK cells remained unchanged (figure 3G). We looked into the gene expression profiles of VeM-treated explants from four patients, and found that many of the overexpressed genes, including *HMGB1*, *CD97*, *MAF*, and *LAMP-3*, could be attributed to the activation of antigen-presenting cells (figure 4A). A similar profile was observed for VeMA-treated patients, but not either paclitaxel or paclitaxel+anti-programmed death ligand 1 (aPD-L1) (online supplemental figure 4A–C). A metascape analysis of the most significantly affected biological pathways following VeM treatment based on the overexpressed genes included: cytokine signaling in the immune system, adaptive immune response, and regulation of mononuclear cell proliferation—suggesting that even with the depletion of T cells, there were still elements important for T-cell response being upregulated (figure 4B). These observations combined with an increase of macrophage-inflammatory protein 1-beta, and IL-17 which are secreted by innate lymphoid cells and monocyte-derived cells (figure 4C), and the elevated expression of LAMP-3 on a larger set of patient samples (online supplemental figure 4D), suggested we focus our investigation on the antigen-presenting cells.

In agreement with our gene expression profiling (figure 3G), we also did not detect a change in the number of antigen-presenting cells (APCs) following venetoclax, metformin, or VeM treatment with flow cytometry (online supplemental figure 4E). However, with established surface marker panels for APCs,^{41 42} we found that metformin clearly increased the proportion of APCs with a potentially more DC-like phenotype (CD11c+, human leukocyte antigen-DR isotype (HLA-DR)+, CD14-) (online supplemental figure 4F,G), which expressed increased levels of CD86 following metformin treatment, hinting that metformin activates these cells (online supplemental figure 4I). To ensure these cells are more likely to be DCs than macrophages, we repeated the experiment with markers of DCs and DC activation,

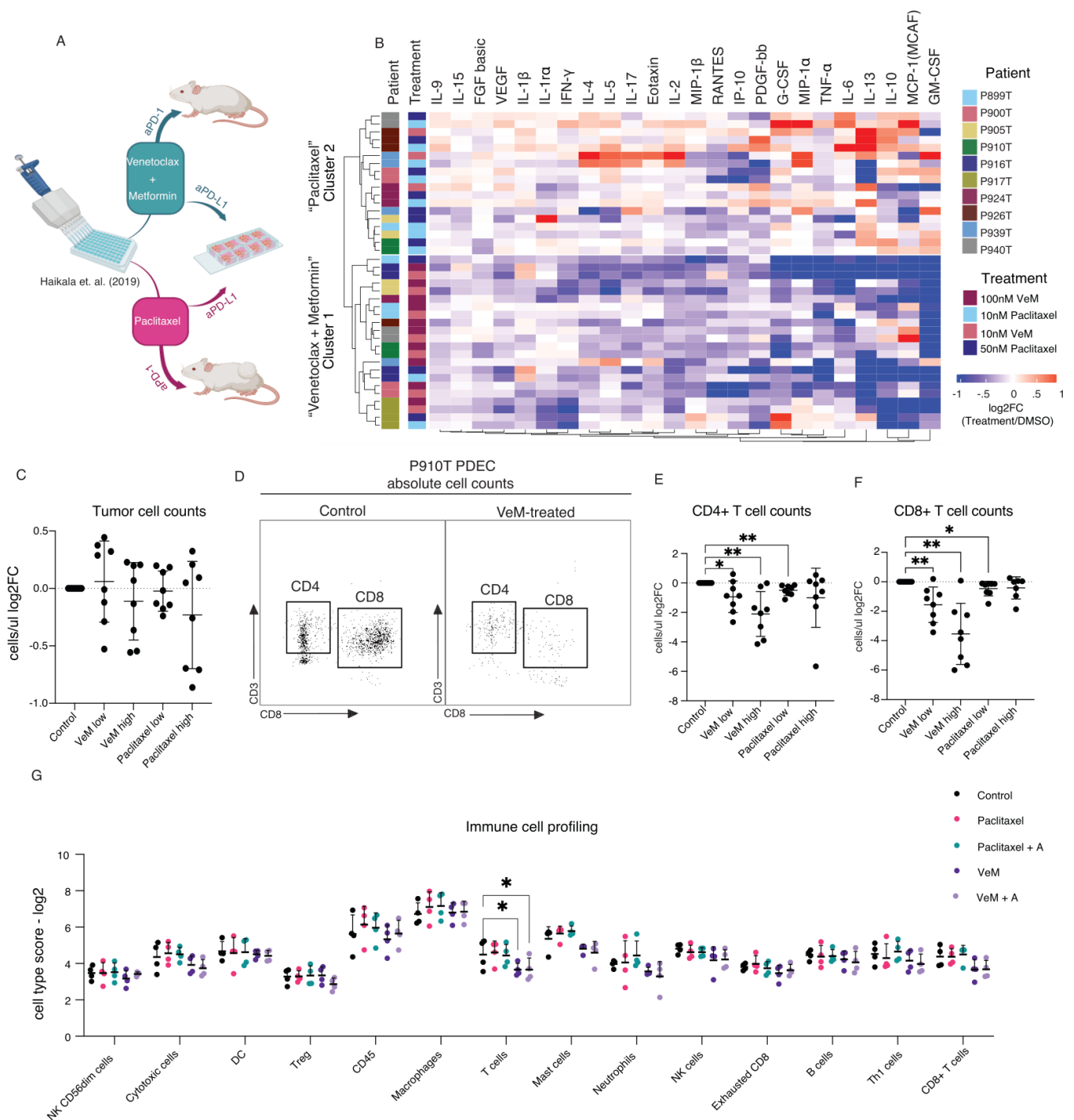


Figure 3 Assessment of combination therapy with venetoclax reveals lymphodepletion of T cells. (A) Schematic summary of the previous finding²⁷ in WAP-Myc mouse model of MYC-driven breast cancer where venetoclax+metformin+aPD-1 treatment in mice resulted in durable antitumor immunity. Here, the VeM treatment along with paclitaxel was profiled in PDECs. (B) Unsupervised hierarchical clustering (Euclidean distance, complete linkage) of PDECs based on cytokine secretion following venetoclax+metformin and paclitaxel treatments (n=10 biologically independent PDECs). (C) CD45- tumor cell viability after VeM or paclitaxel treatments (D) a representative image of quantifying cell viability through flow cytometry for panels (E-F) (E) low (10nM venetoclax+10mM metformin) (p=0.0428) and high (100nM venetoclax+10mM metformin) (p=0.0059) concentrations of VeM negatively impact CD4 T cell viability (CD45+CD3+ CD56 CD4+) (F) low (p=0.0082) and high (p=0.0019) concentrations of VeM negatively impact T effector (CD45+, CD3+, CD56-, CD8+) viability (G) NanoString gene expression profiling of projected cell type scores following treatment of n=4 biologically independent PDECs. High VeM (100 nM venetoclax+10 mM metformin) p=0.0434) without and with aPD-L1 (p=0.0449) negatively impact the T-cell score. Statistical significance was tested with a two-way analysis of variance with Fisher's LSD. All data are presented as mean values \pm SD. aPD-1, anti-programmed cell death 1; aPD-L1, anti-programmed death ligand 1; DC, dendritic cell; DMSO, dimethyl sulfoxide; LSD, least significant difference; NK, natural killer; PDEC, patient-derived explant culture; Treg, regulatory T cell; VeM, venetoclax+metformin.

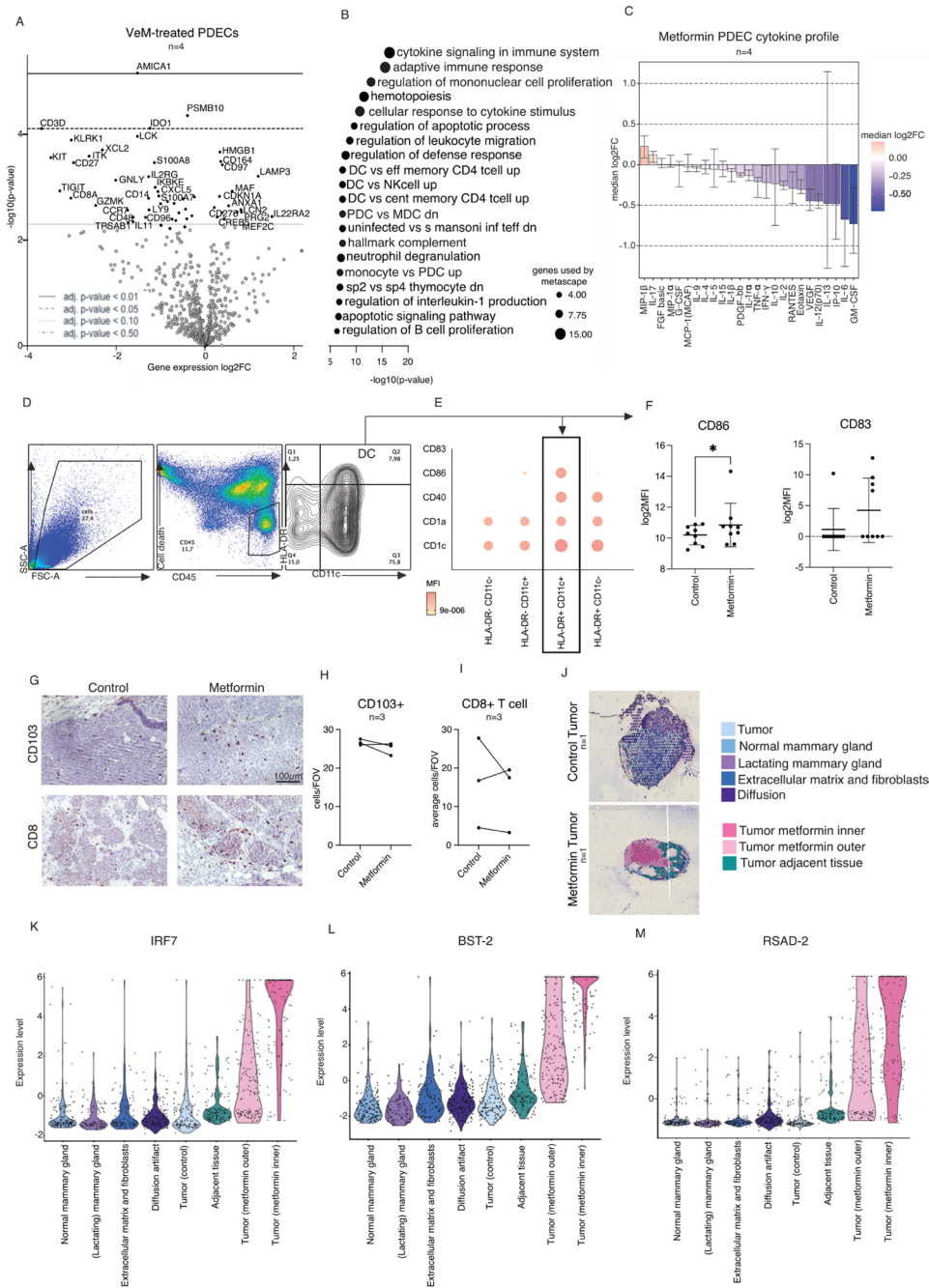


Figure 4 Metformin contributes to dendritic cell activation ex vivo and in vivo. (A) Volcano plot of differentially expressed genes of $n=4$ venetoclax+metformin-treated PDECs. Adjusted p value key described on the plot. (B) Metascape analysis of differentially expressed genes from (A) which are at least 20% upregulated and significant with a p value of <0.05 . The graph depicts terms which were significantly enriched after treatment. Ball size corresponds with the number of genes that overlapped with the gene signatures tested on metascape. (C) Cytokine profiling of PDECs following 10mM metformin treatment. Each cytokine was tested by one-sample non-parametric Wilcoxon test for deviance from 0 (no change) and p values adjusted by FDR method $n=4$. (D) Flow cytometry gating of quadrants with varying expression of HLA-DR and CD11c and (E) the median fluorescence intensity of markers CD1c, CD1a, CD40, CD86 in these four quadrants to determine select antigen-presenting cells with a DC phenotype. (F) CD86 and CD83 expression of dendritic cells following metformin treatment (G) Representative immunohistochemistry staining of CD103 dendritic cell activation marker and CD8 cytotoxic T-cell marker in control and metformin-treated Wap-Myc mouse tumors ($n=3$ control, and $n=3$ metformin-treated mouse tumors). (H–I) Quantification of (G). (J) Control and metformin-treated mouse tumors from Wap-Myc mice with spatial annotations of tissue areas. Each circle is 10 μ m in diameter. (K–M) Mouse DC activation markers, *Bst2*, *Irf7*, and *Rsad2* in varying tumor regions as shown in (J). All data are presented as mean values \pm SD. Statistical significance was tested with a one-way analysis of variance with Fisher's exact test. DC, dendritic cell; FDR, false discovery rate; FOV, field of view; HLA-DR, human leukocyte antigen-DR isotype; MFI, median fluorescence intensity; MDC, myeloid dendritic cell; MFI, median fluorescence intensity; MDC, myeloid dendritic cell; Nk, natural killer; PDEC, patient-derived explant culture; PDC, plasmacytoid dendritic cell.

and found that markers including CD1c, CD1a, CD40, and CD86 could be observed on the surface of the HLA-DR+CD11c+high-expressing cells (figure 4D,E, online supplemental figure 5A). We identify these cells as DCs, although the panel of markers is too limited for definite identification of this cell type. Analysis of these DCs revealed a significant increase in CD86 expression, suggestive of DC activation. Moreover, samples that did not express CD83 began to express DC maturation marker CD83 following metformin treatment (figure 4F). The DC modulation could have positive implications for antitumor immunity, since the predominant role of DCs is to activate T cells, while macrophages clear apoptotic cells and microbes through phagocytosis. Therefore, both the metformin-induced transcriptomic activation of DC activation markers and the increase in the proportion of DC-like cells within the APCs (online supplemental figure 4F,G) were consistent with the idea that metformin could play a role in human DC activation, a notion which has not been made prior to the present study. The remaining APCs, consisting of monocytes and macrophages referred to as mono-macs (CD11c+, HLA-DR+, CD14+), also exhibit a significant decrease in markers associated with immunosuppressive M2 macrophages (online supplemental figure 4F,H) in corroboration to previous mouse studies and human in vitro co-culture studies,^{43–45} which we now extend to authentic ex vivo human tumor tissue cultures.

To explore the effects of metformin in vivo, we investigated Wap-Myc tumor samples from metformin-treated mice for conventional DC (CD103+) and CD8 T cell (CD8+) numbers but found no significant changes in the cells expressing either marker (figure 4G,H,I). These findings were consistent with our findings in PDEC-TIME, where there was an increase in APC activation, but not in overall numbers. Spatial 10x Genomics profiling of Wap-Myc mouse tumor tissue from metformin-treated animals revealed enriched DC activation in metformin-treated mouse compared with control mouse material as determined by the gene expression profiles; metformin increased *Irf7*, *Bst2*, and *Rsad2* expression, while macrophage marker, *CD68*, expression was downmodulated (figure 4J–M; online supplemental figure 5B). Details of how the 10x Genomics and how the tumor areas were classified are explained in supplementary (online supplemental figure 6A). The results from human explants and mouse tumor tissue, treated with venetoclax and metformin (alone or in combination) together suggest that specifically metformin, and not venetoclax, affects DC activation, without altering their numbers.

The mitochondrial respiratory complex I regulates DC activation and DC-mediated activation of CD4+ T-cell proliferation

To determine whether metformin activates APCs directly or through heterotypic cellular interactions, we isolated monocytes from human peripheral blood mononuclear cells (PBMC) of healthy donors. The PBMC-derived

monocytes were then differentiated into either macrophages or DCs. Flow cytometric analysis of macrophages showed that metformin decreased the surface expression of CD163 and CD206 on macrophages differentiated from monocytes with macrophage colony-stimulating factor (M-CSF), markers commonly associated with immunosuppressive macrophages, corroborating publications with similar findings (figure 5A–D).^{44–46} RNA bulk sequencing of metformin-treated monocyte-derived DCs from six donors showed clear evidence for an increase in DC activation (figure 5E, online supplemental figure 7A). Additionally, flow cytometry analysis of monocyte-derived DCs revealed that treatments containing metformin induced a higher proportion of CD86-high, HLA-DR-high activated DCs from the total population (figure 5F,G) suggesting that metformin indeed directly contributes to DC activation. Flow cytometry analysis of DC surface activation markers, and a transcriptional increase in DC activation gene sets suggests a less documented role of DCs as a potential mediator of metformin's antitumor effect in humans.

Metformin is a medicinal biguanide, which acts as a weak inhibitor of mitochondrial respiratory CI (figure 5E).⁴⁷ Inhibition of CI decreases the generation of ATP from oxidative phosphorylation (figure 5E–H, online supplemental figure 8A–C) and the resulting increase in AMP:ATP and ADP:ATP ratios activate adenosine 5'-monophosphate kinase (AMPK), an event commonly observed in metformin-treated cells in vitro and in vivo.^{48–49} To test whether metformin induces DCs activation through activation of AMPK or inhibition of the mitochondrial CI, an experiment was designed to evaluate separately the effect of AMPK-activation, and CI inhibition on DC activation. We found that inhibition of mitochondrial CI with metformin, with the classical CI inhibitor rotenone or with a specific ubiquinone reduction site targeted CI inhibitor IACS-010759⁵⁰ led to an increase in DC activation, whereas direct pharmacological allosteric AMPK activator A-769662 had no noticeable effect (figure 5I). These results suggest that the mechanism by which metformin activates DCs is largely through CI inhibition.

DCs which express elevated levels of activating co-stimulatory signals, including CD86, promote T-cell proliferation and acquisition of their cytotoxic abilities.⁵¹ Thus, we explored whether metformin's effect on DC activation has functional consequences on the activation of T cells. We pretreated DCs with metformin, A-769662, IACS-010759 and rotenone for 48 hours, and then co-cultured the DCs with autologous T cells in the absence of drugs. Importantly, we used anti-CD3 in the co-culture to fulfill the requirement of T cells to not only receive secondary co-stimulatory signals from APCs, but also to have the primary signal through the T-cell receptor which we were supplementing artificially (online supplemental file 8). An increase in CD4+T cell proliferation was quantified as a shift in the proportion of T cells in proliferation (G0=unproliferated T cells, G1=first division, etc),

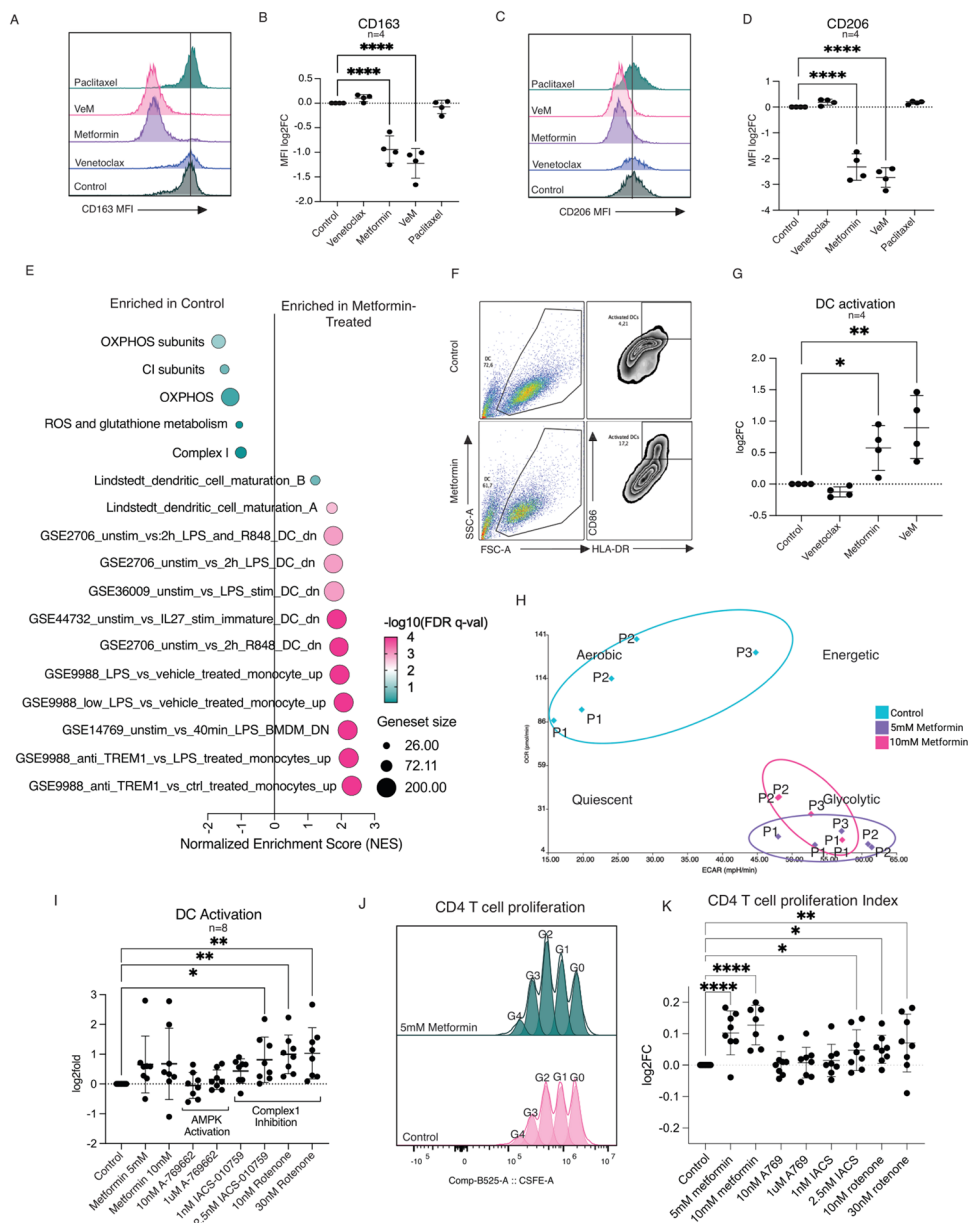


Figure 5 Complex 1 inhibition contributes to DC activation and CD4+T cell proliferation. (A) Representative flow cytometry histogram of median fluorescence intensity of CD163 of monocyte-derived macrophages following treatment. (B) Quantification of (A) from monocyte-derived macrophages of four biologically independent PBMC donors. (C) Representative flow cytometry histogram of median fluorescence intensity of CD206 of monocyte-derived macrophages following treatment. (D) Quantification of (C) from monocyte-derived macrophages of four biologically independent PBMC donors. (E) Gene Set Enrichment Analysis comparison of differentially expressed genes between 10 mM metformin and control-treated PBMC-derived dendritic cells from $n=6$ biologically independent PBMC donors. (F) Flow cytometry gating guide of HLA-DR and CD86 high-expressing DCs which are referred to as “activated DCs”. (G) Quantification of the percentage of activated DCs following treatment from $n=4$ monocyte-derived DC samples with significant increase in surface expression of CD86 and HLA-DR following metformin ($p=0.0226$) and venetoclax+metformin ($p=0.0014$) treatments (H) seahorse extracellular flux assay of monocyte-derived DCs ($n=3$, referred to as P1, P2, P3). Data points with the same label are technical repeats. Data shows that 24 hours metformin treatment shifts the energy requirements of DCs from aerobic to glycolytic. (I) Quantification of DC activation following a larger panel of treatments with significant DC activation following 2.5 nM IACS-010759 ($p=0.0287$), 10 nM rotenone ($p=0.0105$), and 30 nM rotenone ($p=0.0309$) (J) representative T-cell proliferation plot. G0 refers to the undivided generation, with each increasing G number referring to the number of proliferative cycles (K) flow cytometry analysis of CD4+T cell proliferation index indicating the proportion of the proliferating samples that keep proliferating (G1–G4) with significant increases in CD4+T cell proliferation following 5 mM metformin ($p=0.0043$) and 10 nM rotenone ($p=0.0161$) treatments. All data are presented as mean values \pm SD. Statistical significance was tested with a one-way analysis of variance with Fisher’s exact test. DC, dendritic cell; FDR, false discovery rate; FSC-A, forward scatter area; GSEA, gene set enrichment analysis; HLA-DR, human leukocyte antigen- DR isotype; MFI, median fluorescence intensity; PBMC, peripheral blood mononuclear cells; PDEC, patient-derived explant culture; SSC-a, side scatter area.

or in other words, the number of divisions of already-proliferating cells (figure 5J–K). This biologically relevant “proliferation index” clearly showed that the trend in CD4+T helper cell proliferation mirrored the trend in DC activation (figure 5K), suggesting increased co-stimulation of these already-dividing cells. Meanwhile, the “division index”, which is a measure of the total proportion of cells that begin to divide (the ratio of G1-4 to G0), revealed a significant negative impact on overall CD4+T cell proliferation following co-culture with DCs treated with AMPK-activator, A-769662 (online supplemental file 8). This can be a result of AMPK-activation interfering with DC maturation as seen in mice.⁵² The highest dose of metformin negates the increase in overall T-cell proliferation induced by 5 mM metformin, likely due to the increase of metformin’s many modes of action which includes AMPK-activation. An increase in overall proliferating T cells is seen with direct CI inhibition using 10 nM and 30 nM rotenone, suggesting that CI inhibition may also be behind the reason we see an increase with 5 mM metformin. These data suggest that CI inhibition may improve an antigen-specific immune response through the activation of DCs.

DISCUSSION

The importance of targeting tumor cells and exploiting the TIME simultaneously is evident in the increasing number of clinical trials combining targeted therapies or chemotherapies with immunomodulatory compounds.⁵³ However, microenvironmental interactions and heterogeneity within the tumor microenvironment that affect treatment response,^{54–56} can be difficult to model in the laboratory. *In vivo*, animal models may require surrogate, species-specific reagents with different pharmacological properties than the original therapeutic drug. *In vitro*, organoid models capture disease heterogeneity and tumor intrinsic features to some extent but are lacking most immune cell components.^{57–59} Some organoid models are being adapted, for example, to use autologous primary tumor-specific CD8+T cells to screen tumor cell killing in response to increased drug-induced T-cell cytotoxicity.⁶⁰ Although beneficial in terms of throughput, this is limited to CD8+T cell-mediated cytotoxicity. Moreover, using the tumor itself is crucial because antitumor T-cell responses can be tumor site specific, even within the same patient.^{61 62} So, while peripheral blood can be powerful as a predictor of monitoring clinical outcome,⁶³ tumor resident immune cells can be more informative for drug development by capturing the complex tumor-TIME dynamics which can be shaped by the baseline immune composition.⁶⁴ Indeed, there is a clear correlation with the full TIME repertoire and clinical outcome, prompting more attention to models with a more diverse repertoire of autologous tumor immune cells.^{65–68}

Here we explored the opportunities provided by BC PDECs. While organoids can be considered as “reconstruction” models where tumors are dissociated into single

cell components that form new structures, explants are a “deconstruction” of the tumor which capture elements of the original architecture, heterogeneity, and immune cell composition of the tumor—but in smaller pieces. Earlier works show that human *ex vivo* explants from various cancer types retain tumor and stroma components in addition to autologous immune cell populations and can respond to anti-PD-1 depending on the cancer type.^{35 69 70} We deduced through single-cell sequencing, gene expression profiling, flow cytometry, and cytokine profiling of PDECs in comparison to primary tumor material that PDECs also retain all major immune cell subtypes and baseline immune cell activity up to 1 week in culture, which makes these PDEC-TIME cultures an attractive model to explore tumor-TIME dynamics, although this specific model is not optimized for stromal interactions, as these are disrupted during the enzymatic processing of the samples.

While we failed to see an increase in T-cell activity or tumor cell death in BC PDECs in response to either anti-PD-1 or anti-PD-L1, we did see strong immune activation in response to artificial T-cell activation using an anti-CD3/CD28/CD2 tetramer similarly to Voabil (2021), suggesting that T cells within breast tumors lack tumor antigen reactivity. In response to anti-CD3/CD28/CD2, we first observed cell death appearing in PDECs with CellTox staining and an increase in immune activation markers IFN- γ , PRF1, and GZMB via qPCR from bulk RNA. Subsequent flow cytometry and cytokine profiling revealed that the cell death was specifically affecting CD45⁺ tumor cells, while cytokines of T-cell activation (eg, IL-2, IFN- γ , interferon gamma-induced protein 10 (IP-10)) were increased along with T-cell surface expression of checkpoint molecules like PD-1, PD-L1, PD-L2, and LAG-3. Altogether, these findings suggest that with the correct treatment strategy, breast tumor-resident immune cells in PDECs have the potential to be exploited for preclinical antitumor activity.

In our previous work on MYC-driven mouse models of BC, we observed exceptionally durable tumor growth control following a triple-treatment of VeM, and anti-PD-1.²⁷ The *ex vivo* PDEC model, however, revealed a downregulation of all 27 tested cytokines following VeM treatment. Additional flow cytometry data revealed severe T-cell toxicity, especially among CD8+T cytotoxic cells. We attributed this phenomenon to corroborating the lymphotoxic effects of venetoclax on human T cells observed *in vitro* and *in vivo*.^{34 71} Nevertheless, gene expression profiling of a larger repertoire of immune cells revealed that other immune cell subsets were unaffected by VeM in terms of numbers, and that there was a significant increase in genes and cytokines suggestive of APC-activation. The survival and activation of APCs, including macrophages and DCs, is highly interesting since APCs are known to mold the pro-/antitumor properties of TIME, and thus play a role in the efficacy of immune-checkpoint blockade.^{72 73}

Classically activated “M1-like” proinflammatory macrophages have been suggested as a standalone therapeutic

strategy for BC due to their tumoricidal properties,⁷⁴ and a biomarker of increased survival in response to trastuzumab.⁷⁵ Meanwhile, alternatively activated “M2-like” macrophages have been linked to poor prognosis in BC. Metformin has been shown to prevent M2 polarization of macrophages, induce M1 polarization of macrophages, and increase the efficacy of checkpoint inhibition in human and mouse studies.^{44–46 76 77} Extending the previous results, we demonstrate in PDECs that 5 mM–10 mM of metformin directly decreases the proportion of immunosuppressive CD163+M2 like macrophages.

DCs are highly potent APCs that can trigger robust, antigen-specific T-cell activation *in vivo* on maturation, and their increased presence is generally considered a good prognostic marker in BC.^{78 79} Our data show that while metformin does not influence the total number of APCs, it induces a higher proportion of activated DCs in PDECs, and we also observed that metformin promotes DC activation of isolated DCs from human PBMCs. Thus, our data suggests that metformin has a direct DC-activating function, contrary to the idea that DC activation was solely induced through the release of tumor antigens following VeM treatment.

Metformin acts as a weak inhibitor of mitochondrial respiratory CI⁴⁷ and as an AMPK-activator.^{48 49} To investigate how metformin mediates its DC activating function, we explored these two most well-known mechanisms of metformin action. We only observed that the metformin effects on DC activation were phenocopied by respiratory complex I inhibition (CI-i), but not by direct allosteric activation of AMPK. Previous reports have suggested that CI-i of DC precursor monocytes with rotenone inhibits the development of monocytes into immature DCs,⁸⁰ however, to our knowledge metformin’s DC-activating effects mediated via CI-i, shown here, have not been previously reported. If metformin inhibits the differentiation of monocytes to immature DC’s, but also simultaneously promotes DC activation, then what would be the net effect of metformin on the fully physiological TIME of BC? Since the evidence indicates that resident DCs within breast tissue are already in an immature DC state,⁸¹ we propose that CI-i would immediately and beneficially target the tumor resident DCs by increasing tumor-antigen presentation by now-mature DCs. Therefore, adding metformin as an agent to explorative or standard cytotoxic treatments could leverage the tumor-antigen-releasing effects of the cytotoxic component, through simultaneously promoting DC-activation—a concept that should be especially considered in the scope of combination immunotherapies aimed at maintaining drug-induced T-cell responses.

Mechanistically, pharmacological inhibition of CI has a variety of different cell energy metabolism and oxidative stress-related effects, which alone or via additive or synergistic effects could explain the DC activation. While the exact mechanism of how CI-i induces DC maturation remains outside of the scope of the present study, we note that previous study has revealed an increase in DC

maturation and subsequent T-cell activation in response to free oxygen radicals,⁸² which are in some circumstances released in response to respiratory CI-i. As an alternative to the causal role of free oxygen radicals, the DCs may undergo a “metabolic shift” in response to CI-i treatment.^{83–86} DCs undergo a metabolic shift from oxidative phosphorylation to aerobic glycolysis in response to toll-like receptor agonists leading to DC maturation.⁵² As metformin and CI-i decrease oxidative phosphorylation,⁸⁷ it is not inconceivable for a compensatory pathway to take over leading to DC maturation.

In summary, we demonstrate PDEC as a versatile preclinical immuno-oncology model of human TIME that can be easily adapted for a variety of research techniques like single-cell sequencing, and other studies that require the extraction of viable, single cells. Using the PDEC-TIME model, we reveal a hitherto unknown role of metformin for the maturation of APCs, specifically DCs, highlighting the potential clinical translatability of CI-i as means of boosting immunotherapy treatments.

MATERIALS AND METHODS

Cell lines and reagents

Human PBMCs were cultured in Roswell Park Memorial Institute (RPMI) medium supplemented with 10% heat-inactivated fetal bovine serum (FBS) (Biowest), 100 U penicillin–streptomycin (Gibco), and 2 mM L-Glutamine (Gibco). PDECs were cultured in MammoCult (STEMCELL Technologies), and the MammoCult media was supplemented with MammoCult proliferation supplement #05622 (STEMCELL Technologies), 20 µg/mL gentamicin (Sigma), 0.1 µg/mL amphotericin B (Biowest) and 10,000 U/mL penicillin/streptomycin (Lonza). Cells and PDECs were grown in a humidified incubator at 37°C under 5% CO₂, and atmospheric oxygen levels.

PDECs were treated with 25 µl/mL anti-CD3/CD28/CD2 (STEMCELL Technologies), 100 µg/mL atezolizumab (Selleck Chemicals), 50 µg/mL pembrolizumab (MedChem), 10–100 nM Venetoclax (MedChem Express), 5–10 mM metformin (MedChem Express), 10–50 nM paclitaxel (MedChem Express), 1–2.5 nM IACS-010759 (Selleck Chemicals), 10–30 nM rotenone (Sigma-Aldrich), and 10 nM–1 µM A-769662 (Sigma-Aldrich), 100 ng/mL lipopolysaccharide (LPS).

Isolation of biological material and three-dimensional culture

Fresh tissue was obtained from the elective BC surgeries performed at the Helsinki University Central Hospital (online supplemental figure 9A,B) (Ethical permit: 243/13/03/02/2013/TMK02 157 and HUS/2697/2019 approved by the Helsinki University Hospital Ethical Committee). Patients participated in the study by signing an informed consent form. Tissues were collected from tumors. From each tumor, a portion was taken for immunohistochemical, a second portion was frozen at –80°C DNA/RNA/protein analysis, and the remainder was used for the 3D cultures. Explants were produced by

incubating the samples overnight in collagenase A (3 mg/mL; Sigma) containing MammoCult media (STEMCELL Technologies) with gentle shaking (130 rpm) at +37°C. The resulting explants were collected via centrifugation at 353 rcf for 5 min and washed once with 1× phosphate-buffered saline (PBS). Isolated explants were embedded in Cultrex Reduced Growth Factor Basement Membrane Extract, Type 2 (R&D Systems) and plated on 8-Chamber Slides (Thermo Scientific).

Flow cytometry

Explants were harvested by washing the wells twice with 1× PBS, then resuspended in 400 µL +4°C Cultrex Organoid Harvesting Solution (Bio-Techne Sales) and incubated at +4°C with gentle shaking for 30 min. Samples were pipetted onto Falcon round-bottom tubes with cell strainer caps (Corning) and centrifuged at 400 rcf for 5 min at +4°C. Samples were resuspended in 100 µL of flow cytometry staining buffer (1× PBS, 10% heat-inactivated FBS (Gibco)) and the appropriate antibodies (online supplemental table 1) for 45 min at +4°C in the dark. Samples were washed twice with flow cytometry running buffer (1× PBS, 1% heat-inactivated FBS (Gibco)), and resuspended in running buffer for analysis.

Samples were sorted with BD Influx or Sony SH800Z, or analyzed using BD FACSAria II, or NovoCyte Quanteon (Biomedicum Flow Cytometry Unit). Analysis was done using FlowJo V.10.8.1, and graphs were generated using GraphPad Prism V.9.

Flow cytometry antibodies are listed in online supplemental table 1.

Macrophage polarization assay

CD14+ monocytes were isolated using positive magnetic separation with manufacturer instructions (Miltenyi) and were cultured in Iscove's modified Dulbecco's medium (Thermo Fisher) supplemented with 10% heat-inactivated FBS (Gibco), penicillin/streptomycin, and 50 ng/mL human M-CSF (Miltenyi Biotec). Monocytes were plated into 6-well plates (5×10^5 cells) and incubated for 6 days with one medium change. Media from differentiated macrophages was replaced with fresh media containing drugs. The adherent macrophages were detached using macrophage detachment solution DXF (Sigma-Aldrich) for 40 min at +4°C, washed with flow cytometry running buffer, and blocked with Fc-blocking antibody (eBioscience) in flow cytometry running buffer for 10 min at room temperature (according to manufacturer instructions) before adding fluorescent antibodies. Macrophage median fluorescence intensity of surface CD163 and CD206 expression was analyzed on the NovoCyte Quanteon flow cytometer.

Dendritic cell activation assay

CD14+ monocytes were isolated using positive magnetic separation according to manufacturer protocol (Miltenyi Biotec) and cultured in RPMI medium supplemented with 10% heat-inactivated FBS (Biowest), 100 U

penicillin–streptomycin (Gibco), and 2 mM L-Glutamine (Gibco) with added 100 ng/mL Human granulocyte-macrophage colony-stimulating factor (GM-CSF) (Miltenyi Biotec), and 100 ng/mL Human IL-4 (Miltenyi Biotec) for 5 days only adding media once in between. On day 5, DCs were harvested and plated on a 96-well flat-bottom plate. Samples were incubated with 200 µL fresh media containing drugs for 48 hours. DCs were harvested and analyzed using flow cytometry on NovoCyte Quanteon. DCs expressing high levels of HLA-DR and CD86 were considered activated.

T-cell proliferation assay

T cells were isolated using Pan T magnetic isolation beads (Miltenyi Biotec) according to manufacturer protocol, and stained with 1 µM carboxyfluorescein succinimidyl ester (CFSE) in 1× PBS in 37°C 5% CO₂ for 10 min before washing the samples with media. Stained T cells were co-cultured with autologous DCs at a ratio of 5:1 (T:DC) in DC media. 100 ng/mL of Ultra-Leaf purified anti-human CD3 (BioLegend 300413) was added to each sample, and anti-CD3/CD28/CD2, ImmunoCult (STEMCELL Tech) was used as a positive control. Samples were incubated for 72 hours at 37°C 5% CO₂ before being harvested and analyzed using flow cytometry. T-cell proliferation was quantified as the division index and proliferation index as calculated by FlowJo V.10.8.1 software.

Division index: Total number of divisions/the number of cells at the start of the culture.

Proliferation index: Total number of divisions/cells that went into division.

scRNA sequencing and analysis

PDEC samples were harvested and stained with CD45+ to isolate CD45+ leukocytes with fluorescence-activated cell sorting from the total tumor tissue. Up to 30,000 CD45+ cells were collected for single cell 3' v3 library preparation with 10x Genomics Chromium. These single-cell libraries were sequenced on an Illumina NovaSeq 6000. Raw data were demultiplexed, aligned to GRCh38-2020-A and gene count data were generated by Cell Ranger (cellranger-4).

Raw count matrices were further analyzed in Seurat. Barcodes with <20% mtRNA, >400 unique read-counts, and a number of features between 200 and 6,000 were retained as cells.

Next, the data were integrated using Seurat's canonical-correlation-analysis,⁸⁸ clustered and visualized by uniform manifold approximation and projection (UMAP). Cell types were identified based on established marker genes. Significantly enriched cell types between cultured and tissue samples were calculated using the MASC algorithm.⁸⁹ The copy-number variation was assessed with inferCNV (<https://github.com/broadinstitute/inferCNV>) to identify the clusters of cancer cells. Preprocessed data may be found deposited online.⁹⁰

Seahorse extracellular flux assay

CD14⁺ monocytes were isolated using positive magnetic separation according to manufacturer protocol (Miltenyi Biotec) and cultured in RPMI medium supplemented with 10% heat-inactivated FBS (Biowest), 100 U penicillin–streptomycin (Gibco), and 2 mM L-Glutamine (Gibco) with added 100 ng/mL Human GM-CSF (PeproTech), and 10 ng/mL Human IL-4 (PeproTech) for 5 days only adding media once in between. The immature DCs were then treated with either 5 mM or 10 mM metformin for 24 hours. The cells were collected and centrifuged (200 g, 5 min) and resuspended in Agilent RPMI assay medium containing 10 mM glucose (Agilent), 100 mM pyruvate (Agilent), and 200 mM glutamine (Agilent). 50 μ L of cell suspension was pipetted into the Agilent cell culture microplate (Agilent 103794–100) precoated with CellTak (Corning). Cells were centrifuged 200 g, 1 min with no brakes, and then incubated without CO₂ for 25 min as the drug-containing calibration cartridge was calibrating in the Seahorse XFe96. 130 μ L more of assay medium was pipetted per sample, and after another 20 min of incubation with 37°C, no CO₂, the samples were analyzed for metabolic changes following the injection of 1.5 μ M oligomycin (TargetMol), 1 μ M FCCP (TargetMol), 0.5 μ M rotenone (Sigma-Aldrich)+0.5 μ M antimycin (Sigma-Aldrich), and 1:5,000 dilution of Hoechst (Thermo Scientific) using the standard reading frame per injection of 3 min mix, 0 min wait, 3 min measure. The number of technical repeats was based on available cell numbers.

3' RNA sequencing

Total RNA was isolated using RNeasy Plus (Qiagen) which contains a genomic deoxyribonucleic acid (gDNA) eliminator column. RNA sequencing libraries were prepared from 100 ng of total RNA using either the ScriptSeq Complete Gold Kit or the NEBNext Ultra Directional RNA Library Prep Kit for Illumina depending on the RNA integrity. Using the ScriptSeq Complete Gold Kit, the ribosomal RNA was removed first from the total RNA using the Ribo-Zero Gold rRNA Removal Kit after which the RNA was fragmented chemically. The libraries were prepared according to the manufacturer's instructions. Finally, the library was assessed with the Agilent Bioanalyzer.

The NEBNext Ultra Directional RNA Library Prep Kit for Illumina was used to generate the complementary DNA (cDNA) libraries for next-generation sequencing. First, the ribosomal RNA-depleted samples (10 ng) were fragmented to generate the inserts around 200 bp. The libraries were prepared according to the manufacturer's instructions. The library quality was assessed with Bioanalyzer (Agilent DNA High Sensitivity chip) and the library quantity with the Qubit (Invitrogen).

Samples were sequenced with the NextSeq 500—Illumina instrument using 75 Paired-End reads with a sequencing depth of 33 M reads/sample. Differentially expressed genes between different groups were found using state-of-the-art statistical methods and packages,

such as edgeR/DESeq2. The Gene Set Enrichment Analysis (GSEA) V.3.0 (Broad Institute) was used to analyze the differences in the gene expression profiles. GSEA results were visualized using GraphPad Prism V.9.5.0. Data can be found deposited online.⁹⁰

Mouse tissue spatial transcriptomics

Two cryopreserved tumor tissue sections from one metformin-treated and one untreated Wap-Myc mice were profiled for spatial transcriptomics using the 10x Genomics Visium spatial RNA-sequencing technology with a resolution of 55 μ m per spot. The tissues were cryosectioned at 10 μ m thickness onto the Visium library preparation slide, fixed in methanol for 30 min, stained with Hematoxylin and Eosin Stain Kit (Vector Laboratories) and stored at –20°C until library preparation. The slide was imaged using Zeiss Axio Imager.

Sequencing library preparation was performed according to the Visium Spatial Gene Expression user guide (CG000239 RevC, 10x Genomics) using a 12 min tissue-permeabilization time that was tested earlier with the Tissue Optimization Slide to be optimal for the mouse tumor tissues.

Libraries were sequenced with Illumina NovaSeq 6000 sequencer at the FIMM Genomics core facility at the University of Helsinki, with the aimed depth of 75 million reads per section (corresponding to approximately 50,000 reads per tissue-covered array spot).

The analysis was done using R V.4.2.2 and Seurat V.4.3.0. In order to maintain only good quality spots and relevant spots in analysis, spots with lesser than 500 Features or more than 25% of mitochondrial transcripts or more than 1% of hb transcripts were excluded from the analysis. Data was normalized using SCTransform⁹¹ and afterward, principal component analysis and dimension reduction with UMAP⁹² was done with default parameters and with Seurat functions accordingly. Identification of clusters was done with Seurat FindClusters function and a resolution of 0.8. Top significantly (p value adjusted <0.05) differentially expressed genes (online supplemental figure 5C,D) obtained from Seurat FindMarkers function (Wilcoxon rank-sum test) were used for cluster annotation. Differentially expressed genes between different tumor areas were defined by using the same function and Wilcoxon rank-sum test.

NanoString gene expression profiling

Total RNA was isolated using RNeasy (Qiagen), and the DNAase removal step was performed after the isolation (Zymo research). Samples went through QC (Qubit), gene expression analysis was conducted on the NanoString nCounter gene expression platform (NanoString Technologies). Due to the systemic reduction of TILs in explants, the samples were normalized to the genes that create the TIL score: T cell, CD45, B cell, cytotoxic cell, and macrophage genes excluding those with counts below 100 (*CD3G*, *CD3D*, *CD3E*, *SH2D1A*, *CD6*, *PTPRC*, *BLK*, *MS4A1*, *TNGFRSF17*, *CD19*, *CD84*, *CD68*, *CD163*, *CTSW*,

KLRB1, KLRD1, GzMB, PRF1, GZMA, GNLY, KLRK1, GZMH, CD8, CD8A, CD8B, CD4) before comparing activity profiles. Significance was calculated with nSolver's directional significance score calculated as t-statistic for each gene against each covariate in the model, taking the sign of the t-statistics into account.

nCounter Human PanCancer Immune Profiling Panel consisting of 770 genes from different immune cell types, common checkpoint inhibitors, CT antigens, and genes covering both the adaptive and innate immune response. Per sample, 50 ng of total RNA in a final volume of 5 μ L was mixed with a reporter codeset, and hybridization buffer, and capture codeset. Samples were hybridized overnight at 65°C for 20 hours. Hybridized samples were run on the NanoString nCounter SPRINT profiler. Data set found deposited online.⁹⁰

Multiplex and standard immunohistochemistry

Tissues and explant cultures were fixed with 4% paraformaldehyde (PFA) and embedded in paraffin. The samples were sectioned into 5 μ m slices and deparaffinized. The heat-induced antigen retrieval was performed with a microwave oven or a pressure cooker in a citrate buffer solution (Dako). Histochemical stainings were carried out using standard techniques for IHC and IHC-IF. Images were taken with a Leica DM LB microscope or with a Zeiss AxioImager 1 (Biomedicum Imaging Unit, University of Helsinki). Multiplex images were stained in two rounds and tissue sections were scanned on the Zeiss AxioImager Z1 scanner at FL20X.

The list of used antibodies is shown in online supplemental table 2.

Immunofluorescent staining

3D cultured BC explants were fixed with 4% PFA for 15 min at room temperature and washed three times with PBS. The tissue explants were permeabilized with 0.5% Triton X-100 in PBS for 10 min at room temperature (RT) and blocked in an IF buffer (0.1% BSA, 0.2% Triton X-100, 7.7 mM NaN₃, and 0.05% Tween 20 in PBS) supplemented with 10% (v/v) normal goat serum for 1 hour. Explants were then incubated with the primary antibody diluted in a blocking solution overnight at 4°C. Following incubation, explants were washed three times with an IF buffer and then incubated using the appropriate Alexa Fluor secondary antibody diluted in an IF buffer with 10% goat serum. After 60 min of incubation at RT, the explants were washed with an IF buffer as before and the nuclei were counterstained with Hoechst 33258 (Sigma). Instead of antibodies, cell death staining was done with the CellTox green (Promega) at a dilution of 0.25 μ L CellTox/500 μ L media for 20 min. Samples were then washed twice with 1 \times PBS, fixed with 2% PFA for 20 min, washed twice with 1 \times PBS, and stored in +4°C until imaging. Slides containing tissue explants were mounted with the ImmuMount reagent (Fisher Scientific). Images of the structures were acquired using a Leica TCS SP8 CARS confocal microscope using an HC PL APO CS2

40 \times objective (Biomedicum Imaging Unit, University of Helsinki).

Cytokine profiling

PDEC cytokine secretion was analyzed from cleared PDEC culture supernatants using Bio-Plex Pro Human Cytokine 27-plex assay kit (Bio-Rad, cat. M500KCAF0Y) and Bio-Plex 200 System (Bio-Rad) according to the manufacturer's instructions. Results were analyzed using Bio-Plex Manager V.6.0 software (Bio-Rad Laboratories).

Cytokines with >10% of data points outside the detection range were excluded from the analyses. Remaining values lower than the detection limit were replaced by 0.5' lowest measured value. Further data analyses and visualizations were performed using R (V.4.0.4,⁹³ tidyverse V.1.3.1). To identify changes in untreated PDEC cytokine secretion over time, we calculated \log_2 foldchanges between day 6 and day 3 cytokine levels and analyzed their deviance from 0 (unchanged) with one-sample t-test. The resulting Benjamini-Hochberg-adjusted p values and average \log_2 foldchanges were visualized as a volcano plot. For comparing different treatments, we used dimethyl sulfoxide (DMSO)-treated PDEC cytokine levels as a baseline and calculated \log_2 foldchanges for the indicated treatments. Unsupervised hierarchical clustering was performed with R (function hclust) based on \log_2 foldchanges and visualized as a heatmap using ComplexHeatmap package (V.2.6.2).⁹⁴ Bar graphs (median \pm IQR) and line plots (median) were plotted using \log_2 foldchange values, and statistical significances were reported as Benjamini-Hochberg adjusted p values from one-sample Wilcoxon signed-rank tests (deviance from zero).

q-PCR analysis

Total RNA was isolated from cell lines and primary cell cultures using the Qiagen RNEasy Kit according to the manufacturer's instructions, while the cDNA synthesis was performed with the Maxima First Strand cDNA Synthesis Kit for real-time quantitative polymerase chain reaction (RT-qPCR) (Thermo Scientific). RT-qPCR was performed with LightCycler 480 II (Roche) using DyNAmo Color-Flash SYBR Green (Thermo Scientific). The gene-specific primer sets were used at a final concentration of 0.2 mM.

Primers are listed in online supplemental table 3.

Statistical analysis

We report our results as the mean \pm SD. Data sets were analyzed using Fisher's exact test. All the experiments with representative images (immunohistology, and immunofluorescence stainings) have been repeated at least thrice. When comparing multiple groups, the p values were calculated using one-way analysis of variance, unless otherwise specified in the figure legend.

Author affiliations

¹Translational Cancer Medicine, University of Helsinki, Helsinki, Finland

²University of Turku, Turku, Finland

³KU Leuven, Leuven, Belgium

⁴Department of Human Genetics, KU Leuven, Leuven, Belgium

⁵University of Helsinki Faculty of Medicine, Helsinki, Finland

⁶Scellex, Helsinki, Finland

⁷Department of Pathology, Helsinki University Central Hospital, Helsinki, Finland

⁸Department of Pathology, HUSLAB, Helsinki University Central Hospital, Helsinki, Finland

⁹Breast Surgery Unit, Helsinki University Central Hospital Comprehensive Cancer Center, Helsinki, Finland

¹⁰Department of oncology, Helsinki University Central Hospital, Helsinki, Finland

¹¹TRIMM, Translational Immunology Research Program, University of Helsinki, Helsinki, Finland

¹²University of Helsinki Helsinki Institute of Life Sciences, Helsinki, Finland

¹³Department of Cell & Tissue Biology, UCSF, San Francisco, California, USA

¹⁴VIB–KU Leuven Center for Cancer Biology, Leuven, Belgium

¹⁵Finnish Cancer Institute, Helsinki, Finland

X Rita Turpin @CancerResearch, Satu Mustjoki @hruh_research and Juha Klefström @KlefstromLab

Acknowledgements We are grateful to the patients who participated in this research by donating breast tumor tissue samples and made it possible, and to the surgical personnel at Helsinki University Hospital who assisted with the recruitment and collection of the sample material. We are grateful to Biomedicum Imaging Unit (BIU), Biomedicum Functional Genomics Unit (FuGU), and Biomedicum Flow Cytometry Unit (from HiLIFE, University of Helsinki and Biocenter Finland) for their services. We thank the Klefström laboratory personnel for discussions and critical comments on the manuscript. Schematic images were created with BioRender.com. We thank the Finnish Cancer Institute (FCI) for financial support.

Contributors RT and JK wrote the paper, conceived and designed the analysis. MH, JP, DL, AG, PS, SM and MM conceived and designed the analysis, data analysis and interpretation. RT, RL, PMM, AP, JHR, GP, BB, NS, EH, IS, JA, EMV, LL and MM collected the data, contributed data and analysis tools. JM, TM, LN and PK collected the data. JK is the guarantor of this study.

Funding This work was supported by grants from the Academy of Finland, Business Finland, the Finnish Cancer Organizations, Sigrid Juséliuksen Säätiö, Jane and Aatos Erkon Säätiö, the Research Council of Finland, and RESCUER project, which has received funding from the European Union's Horizon 2020 Framework Programme (no. 847912). This work was also supported by the US Department of Defense for Health Affairs through the Breast Cancer Research Program under (award no. W81XWH2110773). Opinions, interpretations, conclusions, and recommendations are those of the author and are not necessarily endorsed by the Department of Defense. In addition, funds were received from Sihtasutus Archimedes, Ida Montinin Säätiö, Finnish Cancer Institute, Syöpäjärjestöt, and the iCAN Digital Precision Cancer Medicine Flagship.

Competing interests MH is an employee, owns shares and has received research funding from Faron Pharmaceuticals.

Patient consent for publication Not applicable.

Ethics approval Fresh tissue was obtained from the elective breast cancer surgeries performed at the Helsinki University Central Hospital (Ethical permit: 243/13/03/02/2013/ TMK02 157 and HUS/2697/2019 approved by the Helsinki University Hospital Ethical Committee). Participants gave informed consent to participate in the study before taking part.

Provenance and peer review Not commissioned; externally peer reviewed.

Data availability statement Data are available upon reasonable request. Source data for BRB sequencing, scSequencing, and gene expression profiling can be found deposited at <https://doi.org/10.5281/zenodo.7906989> under the Creative Commons Attribution 4.0 International license. All other manuscript data are available from the authors upon reasonable request. All data relevant to the study are included in the article or uploaded as supplementary information.

Supplemental material This content has been supplied by the author(s). It has not been vetted by BMJ Publishing Group Limited (BMJ) and may not have been peer-reviewed. Any opinions or recommendations discussed are solely those of the author(s) and are not endorsed by BMJ. BMJ disclaims all liability and responsibility arising from any reliance placed on the content. Where the content includes any translated material, BMJ does not warrant the accuracy and reliability of the translations (including but not limited to local regulations, clinical guidelines,

terminology, drug names and drug dosages), and is not responsible for any error and/or omissions arising from translation and adaptation or otherwise.

Open access This is an open access article distributed in accordance with the Creative Commons Attribution Non Commercial (CC BY-NC 4.0) license, which permits others to distribute, remix, adapt, build upon this work non-commercially, and license their derivative works on different terms, provided the original work is properly cited, appropriate credit is given, any changes made indicated, and the use is non-commercial. See <http://creativecommons.org/licenses/by-nc/4.0/>.

ORCID iDs

Satu Mustjoki <http://orcid.org/0000-0002-0816-8241>

Juha Klefström <http://orcid.org/0000-0001-7124-8431>

REFERENCES

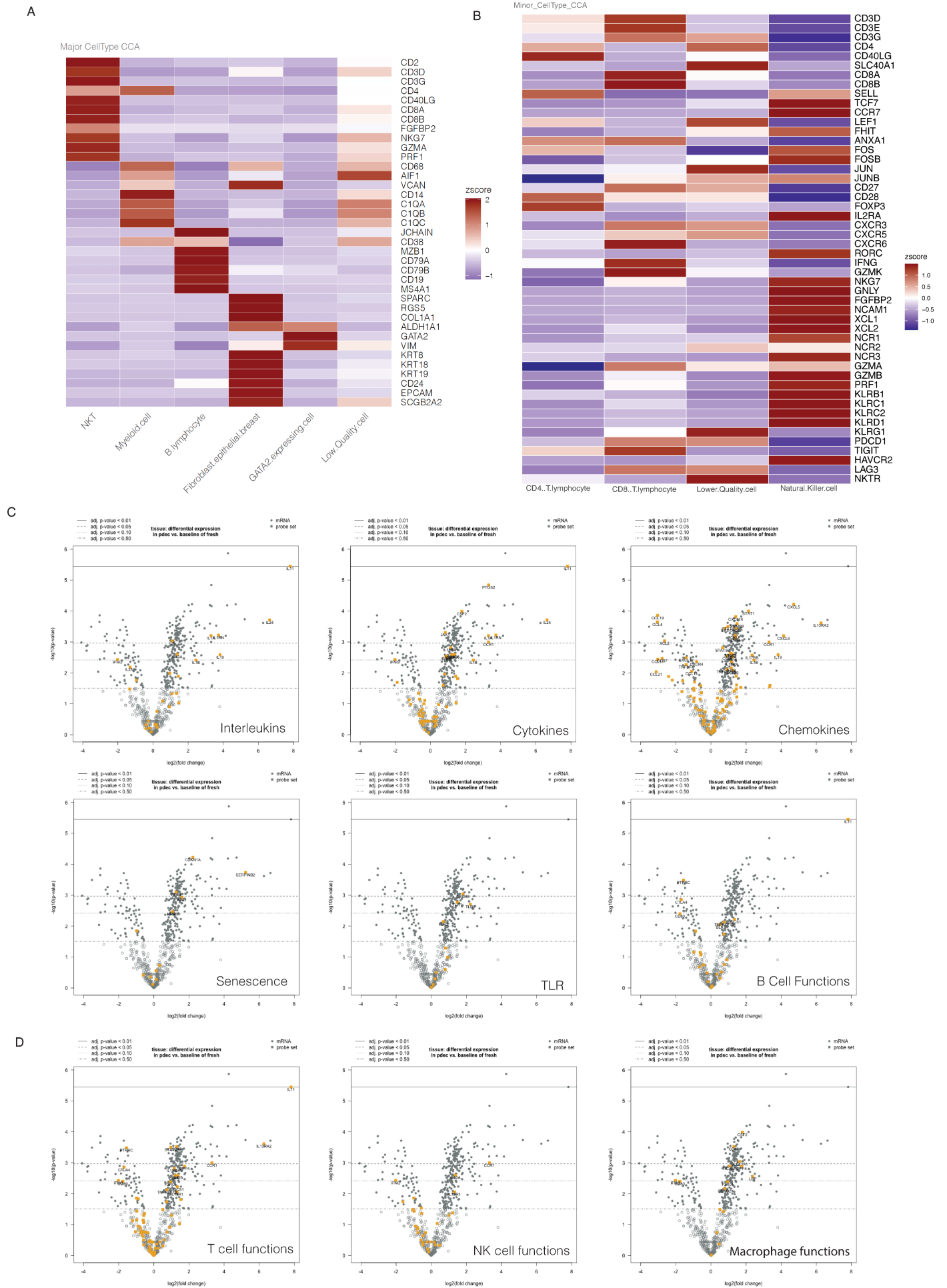
- Chen DS, Mellman I. Elements of cancer immunity and the cancer-immune set point. *Nature* 2017;541:321–30.
- Ye Y, Zhang Y, Yang N, *et al.* Profiling of immune features to predict immunotherapy efficacy. *Innovation (Camb)* 2022;3:100194.
- Chen DS, Mellman I. Oncology meets immunology: the cancer-immunity cycle. *Immunity* 2013;39:1–10.
- Sharma P, Allison JP. Immune checkpoint targeting in cancer therapy: toward combination strategies with curative potential. *Cell* 2015;161:205–14.
- Mackall CL, Fleisher TA, Brown MR, *et al.* Lymphocyte depletion during treatment with intensive chemotherapy for cancer. *Blood* 1994;84:2221–8.
- Verma R, Foster RE, Horgan K, *et al.* Lymphocyte depletion and repopulation after chemotherapy for primary breast cancer. *Breast Cancer Res* 2016;18:10.
- Ruffell B, Coussens LM. Macrophages and therapeutic resistance in cancer. *Cancer Cell* 2015;27:462–72.
- Shree T, Olson OC, Elie BT, *et al.* Macrophages and cathepsin proteases blunt chemotherapeutic response in breast cancer. *Genes Dev* 2011;25:2465–79.
- Rugo HS, Delord J-P, Im S-A, *et al.* Safety and antitumor activity of Pembrolizumab in patients with estrogen receptor–positive/human epidermal growth factor receptor 2–negative advanced breast cancer. *Clin Cancer Res* 2018;24:2804–11.
- Dirix LY, Takacs I, Jerusalem G, *et al.* Avelumab, an anti-PD-L1 antibody, in patients with locally advanced or metastatic breast cancer: a phase 1B JAVELIN solid tumor study. *Breast Cancer Res Treat* 2018;167:671–86.
- Adams S, Loi S, Toppmeyer D, *et al.* Pembrolizumab monotherapy for previously untreated, PD-L1–positive, metastatic triple-negative breast cancer: cohort B of the phase II KEYNOTE-086 study. *Ann Oncol* 2019;30:405–11.
- Ademuyiwa FO, Gao F, Chen I, *et al.* Abstract PD14-09: NCI 10013 – A randomized phase 2 study of neoadjuvant carboplatin and paclitaxel, with or without Atezolizumab in triple negative breast cancer (TNBC). *Cancer Res* 2021;81:PD14–09.
- Schmid P, Rugo HS, Adams S, *et al.* Atezolizumab plus NAB-paclitaxel as first-line treatment for Unresectable, locally advanced or metastatic triple-negative breast cancer (Impassion130): updated efficacy results from a randomised, double-blind, placebo-controlled, phase 3 trial. *Lancet Oncol* 2020;21:44–59.
- Upadhaya S, Neftelino ST, Hodge JP, *et al.* Combinations take centre stage in PD1/PDL1 inhibitor clinical trials. *Nat Rev Drug Discov* 2021;20:168–9.
- Lv B, Wang Y, Ma D, *et al.* Immunotherapy: reshape the tumor immune microenvironment. *Front Immunol* 2022;13:844142.
- De Henau O, Rausch M, Winkler D, *et al.* Overcoming resistance to checkpoint blockade therapy by targeting PI3Kγ in myeloid cells. *Nature* 2016;539:443–7.
- O'Neil NJ, Bailey ML, Hieter P. Synthetic lethality and cancer. *Nat Rev Genet* 2017;18:613–23.
- Dang CV. MYC on the path to cancer. *Cell* 2012;149:22–35.
- Nieminen AJ, Partanen JI, Hau A, *et al.* c-Myc primed mitochondria determine cellular sensitivity to TRAIL-induced apoptosis. *EMBO J* 2007;26:1055–67.
- Pelengaris S, Khan M, Evan G. c-Myc: more than just a matter of life and death. *Nat Rev Cancer* 2002;2:764–76.
- Juin P, Hunt A, Littlewood T, *et al.* C-Myc functionally cooperates with BAX to induce apoptosis. *Mol Cell Biol* 2002;22:6158–69.
- Klefstrom J, Arighi E, Littlewood T, *et al.* Induction of TNF-sensitive cellular phenotype by c-Myc involves P53 and impaired NF-KB activation. *EMBO J* 1997;16:7382–92.

- 23 Thng DKH, Toh TB, Chow EKH. Capitalizing on synthetic lethality of MYC to treat cancer in the digital age. *Trends Pharmacol Sci* 2021;42:166–82.
- 24 Donati G, Amati B. MYC and therapy resistance in cancer: risks and opportunities. *Mol Oncol* 2022;16:3828–54.
- 25 Horuchi D, Anderton B, Goga A. Taking on challenging targets: making Myc druggable. *Am Soc Clin Oncol Educ Book* 2014:e497–502.
- 26 Souers AJ, Levenson JD, Boghaert ER, et al. ABT-199, a potent and selective BCL-2 inhibitor, achieves antitumor activity while sparing platelets. *Nat Med* 2013;19:202–8.
- 27 Haikala HM, Anttila JM, Marques E, et al. Pharmacological reactivation of MYC-dependent apoptosis induces susceptibility to anti-PD-1 Immunotherapy. *Nat Commun* 2019;10:620.
- 28 Eikawa S, Nishida M, Mizukami S, et al. Immune-mediated antitumor effect by type 2 diabetes drug, metformin. *Proc Natl Acad Sci U S A* 2015;112:1809–14.
- 29 Cha J-H, Yang W-H, Xia W, et al. Metformin promotes antitumor immunity via Endoplasmic-Reticulum-associated degradation of PD-L1. *Mol Cell* 2018;71:606–20.
- 30 Zhang Z, Li F, Tian Y, et al. Metformin enhances the antitumor activity of CD8+ T lymphocytes via the AMPK–miR-107–Eomes–PD-1 pathway. *J Immunol* 2020;204:2575–88.
- 31 Al-Akhrass H, Pietilä M, Lilja J, et al. Sortilin-related receptor is a druggable therapeutic target in breast cancer. *Mol Oncol* 2022;16:116–29.
- 32 Munne PM, Martikainen L, Rätty I, et al. Compressive stress-mediated P38 activation required for ER α + phenotype in breast cancer. *Nat Commun* 2021;12:6967.
- 33 Tervonen TA, Belitškin D, Pant SM, et al. Deregulated Hepsin protease activity confers Oncogenicity by concomitantly augmenting HGF/MET signalling and disrupting epithelial cohesion. *Oncogene* 2016;35:1832–46.
- 34 Kohlhapp FJ, Haribhai D, Mathew R, et al. Venetoclax increases intratumoral effector T cells and antitumor efficacy in combination with immune checkpoint blockade. *Cancer Discov* 2021;11:68–79.
- 35 Voabil P, de Bruijn M, Roelofs LM, et al. An ex vivo tumor fragment platform to dissect response to PD-1 blockade in cancer. *Nat Med* 2021;27:1250–61.
- 36 Voskoboinik I, Dunstone MA, Baran K, et al. Perforin: structure, function, and role in human immunopathology. *Immunol Rev* 2010;235:35–54.
- 37 Shankaran V, Ikeda H, Bruce AT, et al. IFN γ and lymphocytes prevent primary tumour development and shape tumour immunogenicity. *Nature* 2001;410:1107–11.
- 38 Sabat R, Grütz G, Warszawska K, et al. Biology of Interleukin-10. *Cytokine Growth Factor Rev* 2010;21:331–44.
- 39 Malek TR. The biology of Interleukin-2. *Annu Rev Immunol* 2008;26:453–79.
- 40 Urbaniak A, Piña-Oviedo S, Yuan Y, et al. Limitations of an ex vivo breast cancer model for studying the mechanism of action of the anticancer drug paclitaxel. *Eur J Pharmacol* 2021;891:173780.
- 41 Gerhard GM, Bill R, Messemaker M, et al. Tumor-infiltrating Dendritic cell states are conserved across solid human cancers. *J Exp Med* 2021;218:e20200264.
- 42 Michea P, Noël F, Zakine E, et al. Adjustment of Dendritic cells to the breast-cancer microenvironment is subset specific. *Nat Immunol* 2018;19:885–97.
- 43 Uehara T, Eikawa S, Nishida M, et al. Metformin induces CD11B+ Cell-mediated growth inhibition of an osteosarcoma: implications for metabolic reprogramming of myeloid cells and anti-tumor effects. *Int Immunol* 2019;31:187–98.
- 44 Chiang C-F, Chao T-T, Su Y-F, et al. Metformin-treated cancer cells modulate macrophage polarization through AMPK-NF-KB signaling. *Oncotarget* 2017;8:20706–18.
- 45 Ding L, Liang G, Yao Z, et al. Metformin prevents cancer metastasis by inhibiting M2-like polarization of tumor associated macrophages. *Oncotarget* 2015;6:36441–55.
- 46 Wang J-C, Sun X, Ma Q, et al. Metformin's antitumor and anti-angiogenic activities are mediated by skewing macrophage polarization. *J Cell Mol Med* 2018;22:3825–36.
- 47 Bridges HR, Blaza JN, Yin Z, et al. Structural basis of mammalian respiratory complex I inhibition by medicinal Biguanides. *Science* 2023;379:351–7.
- 48 Zhou G, Myers R, Li Y, et al. Role of AMP-activated protein kinase in mechanism of metformin action. *J Clin Invest* 2001;108:1167–74.
- 49 Vancura A, Bu P, Bhagwat M, et al. Metformin as an anticancer agent. *Trends Pharmacol Sci* 2018;39:867–78.
- 50 Tsuji A, Akao T, Masuya T, et al. IACS-010759, a potent inhibitor of glycolysis-deficient hypoxic tumor cells, inhibits mitochondrial respiratory complex I through a unique mechanism. *J Biol Chem* 2020;295:7481–91.
- 51 Nurieva R, Thomas S, Nguyen T, et al. T-cell tolerance or function is determined by combinatorial costimulatory signals. *EMBO J* 2006;25:2623–33.
- 52 Krawczyk CM, Holowka T, Sun J, et al. Toll-like receptor-induced changes in glycolytic metabolism regulate Dendritic cell activation. *Blood* 2010;115:4742–9.
- 53 Upadhaya S, Neftelinov ST, Hodge J, et al. Challenges and opportunities in the PD1/PDL1 inhibitor clinical trial landscape. *Nat Rev Drug Discov* 2022;21:482–3.
- 54 Palucka AK, Coussens LM. The basis of Oncoimmunology. *Cell* 2016;164:1233–47.
- 55 Klemm F, Joyce JA. Microenvironmental regulation of therapeutic response in cancer. *Trends Cell Biol* 2015;25:198–213.
- 56 Junttila MR, de Sauvage FJ. Influence of tumour micro-environment heterogeneity on therapeutic response. *Nature* 2013;501:346–54.
- 57 Bhatia S, Kramer M, Russo S, et al. Patient-derived triple-negative breast cancer Organoids provide robust model systems that recapitulate tumor intrinsic characteristics. *Cancer Res* 2022;82:1174–92.
- 58 Sachs N, de Ligt J, Kopper O, et al. A living Biobank of breast cancer organoids captures disease heterogeneity. *Cell* 2018;172:373–86.
- 59 Dekkers JF, van Vliet EJ, Sachs N, et al. Long-term culture, genetic manipulation and Xenotransplantation of human normal and breast cancer Organoids. *Nat Protoc* 2021;16:1936–65.
- 60 Zhou Z, Van der Jeught K, Fang Y, et al. An Organoid-based screen for epigenetic inhibitors that stimulate antigen presentation and potentiate T-cell-mediated cytotoxicity. *Nat Biomed Eng* 2021;5:1320–35.
- 61 Van den Eynde M, Mlecnik B, Bindea G, et al. The link between the multiverse of immune microenvironments in metastases and the survival of colorectal cancer patients. *Cancer Cell* 2018;34:1012–26.
- 62 Hirata E, Sahai E. Tumor microenvironment and differential responses to therapy. *Cold Spring Harb Perspect Med* 2017;7:a026781.
- 63 Hwang M, Canzoniero JV, Rosner S, et al. Peripheral blood immune cell dynamics reflect antitumor immune responses and predict clinical response to immunotherapy. *J Immunother Cancer* 2022;10:e004688.
- 64 Anderson KG, Stromnes IM, Greenberg PD. Obstacles posed by the tumor microenvironment to T cell activity: a case for synergistic therapies. *Cancer Cell* 2017;31:311–25.
- 65 Hegde PS, Karanikas V, Evers S. The where, the when, and the how of immune monitoring for cancer immunotherapies in the era of checkpoint inhibition. *Clin Cancer Res* 2016;22:1865–74.
- 66 Herbst RS, Soria J-C, Kowanetz M, et al. Predictive correlates of response to the anti-PD-L1 antibody MPDL3280A in cancer patients. *Nature* 2014;515:563–7.
- 67 Sharma P, Allison JP. The future of immune checkpoint therapy. *Science* 2015;348:56–61.
- 68 Galon J, Bruni D. Approaches to treat immune hot, altered and cold tumours with combination immunotherapies. *Nat Rev Drug Discov* 2019;18:197–218.
- 69 Yuki K, Cheng N, Nakano M, et al. Organoid models of tumor immunology. *Trends Immunol* 2020;41:652–64.
- 70 Jenkins RW, Aref AR, Lizotte PH, et al. Ex vivo profiling of PD-1 blockade using organotypic tumor spheroids. *Cancer Discov* 2018;8:196–215.
- 71 Lu P, Fleischmann R, Curtis C, et al. Safety and pharmacodynamics of Venetoclax (ABT-199) in a randomized single and multiple ascending dose study in women with systemic lupus erythematosus. *Lupus* 2018;27:290–302.
- 72 Kim IS, Gao Y, Welte T, et al. Immuno-subtyping of breast cancer reveals distinct myeloid cell profiles and immunotherapy resistance mechanisms. *Nat Cell Biol* 2019;21:1113–26.
- 73 Barry KC, Hsu J, Broz ML, et al. A natural killer–Dendritic cell axis defines checkpoint therapy-responsive tumor microenvironments. *Nat Med* 2018;24:1178–91.
- 74 Gabrilovich DI, Ostrand-Rosenberg S, Bronte V. Coordinated regulation of myeloid cells by tumours. *Nat Rev Immunol* 2012;12:253–68.
- 75 Honkanen TJ, Tikkanen A, Karihtala P, et al. Prognostic and predictive role of tumour-associated macrophages in Her2 positive breast cancer. *Sci Rep* 2019;9:10961.
- 76 Wei Z, Zhang X, Yong T, et al. Boosting anti-PD-1 therapy with metformin-loaded macrophage-derived microparticles. *Nat Commun* 2021;12:440.
- 77 Giles ED, Jindal S, Wellberg EA, et al. Metformin inhibits stromal aromatase expression and tumor progression in a rodent model of postmenopausal breast cancer. *Breast Cancer Res* 2018;20:50.
- 78 Hillenbrand EE, Neville AM, Coventry BJ. Immunohistochemical localization of CD1A-positive putative Dendritic cells in human breast tumours. *Br J Cancer* 1999;79:940–4.

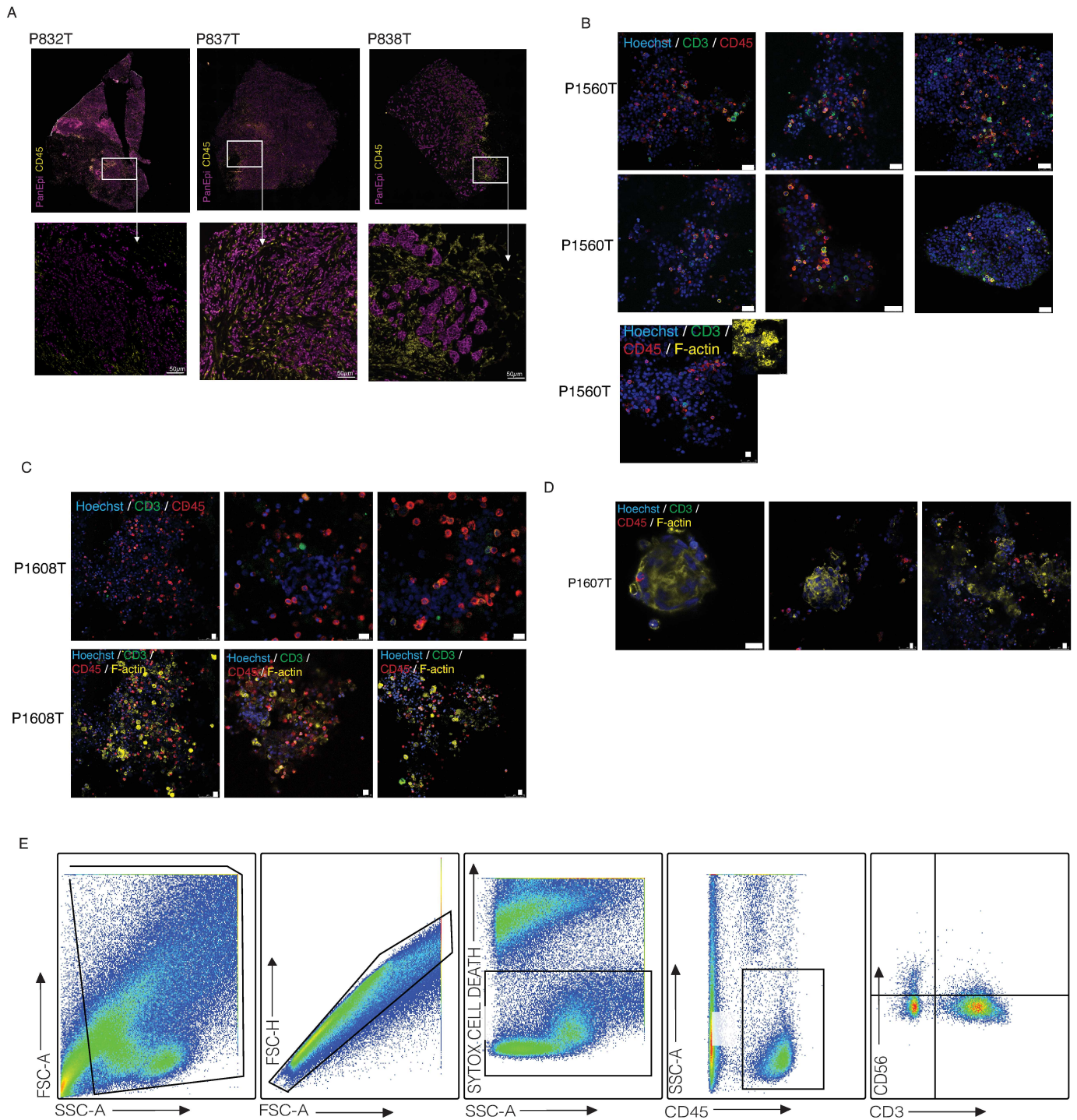


- 79 La Rocca G, Anzalone R, Corrao S, *et al.* CD1A down-regulation in primary invasive Ductal breast carcinoma may predict regional lymph node invasion and patient outcome. *Histopathology* 2008;52:203–12.
- 80 Fato R, Bergamini C, Bortolus M, *et al.* Differential effects of mitochondrial complex I inhibitors on production of reactive oxygen species. *Biochimica et Biophysica Acta (BBA) - Bioenergetics* 2009;1787:384–92.
- 81 Bell D, Chomarat P, Broyles D, *et al.* In breast carcinoma tissue, immature Dendritic cells reside within the tumor, whereas mature Dendritic cells are located in peritumoral areas. *J Exp Med* 1999;190:1417–26.
- 82 Rutault K, Alderman C, Chain BM, *et al.* Reactive oxygen species activate human peripheral blood Dendritic cells. *Free Radic Biol Med* 1999;26:232–8.
- 83 Santos PM, Menk AV, Shi J, *et al.* Tumor-derived A-Fetoprotein suppresses fatty acid metabolism and oxidative phosphorylation in Dendritic cells. *Cancer Immunol Res* 2019;7:1001–12.
- 84 O'Neill LAJ, Pearce EJ. Immunometabolism governs Dendritic cell and macrophage function. *J Exp Med* 2016;213:15–23.
- 85 Liu P-S, Chen Y-T, Li X, *et al.* CD40 signal rewires fatty acid and Glutamine metabolism for stimulating macrophage anti-tumorigenic functions. *Nat Immunol* 2023;24:452–62.
- 86 Du X, Chapman NM, Chi H. Emerging roles of cellular metabolism in regulating Dendritic cell subsets and function. *Front Cell Dev Biol* 2018;6:152.
- 87 Foretz M, Guigas B, Bertrand L, *et al.* Metformin: from mechanisms of action to therapies. *Cell Metab* 2014;20:953–66.
- 88 Diemer J, Kelly M, Kwon EM, *et al.* Single cell RNA-sequencing to uncover cell type-specific gene expression changes during Inv(16) leukemia initiation. *Blood* 2018;132:1326.
- 89 Fonseka CY, Rao DA, Teslovich NC, *et al.* Mixed-effects association of single cells identifies an expanded effector CD4+ T cell subset in rheumatoid arthritis. *Sci Transl Med* 2018;10:eaq0305.
- 90 Turpin R, Liu R, Munne PM, *et al.* Respiratory complex I regulates Dendritic cell maturation in explant model of human tumor immune microenvironment. *bioRxiv* [Preprint] 2023.
- 91 Hafemeister C, Satija R. Normalization and variance stabilization of single-cell RNA-Seq data using regularized negative binomial regression. *Genome Biol* 2019;20:296.
- 92 Bro R, Smilde AK. Principal component analysis. *Anal Methods* 2014;6:2812–31.
- 93 R Core Team. R: A language and environment for statistical computing. *R Foundation for Statistical Computing* [Preprint] 2021.
- 94 Gu Z, Eils R, Schlesner M. Complex heatmaps reveal patterns and correlations in multidimensional genomic data. *Bioinformatics* 2016;32:2847–9.

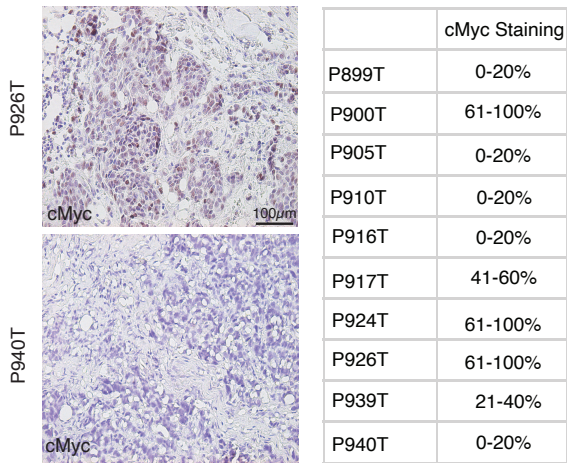
Supplementary Fig 1



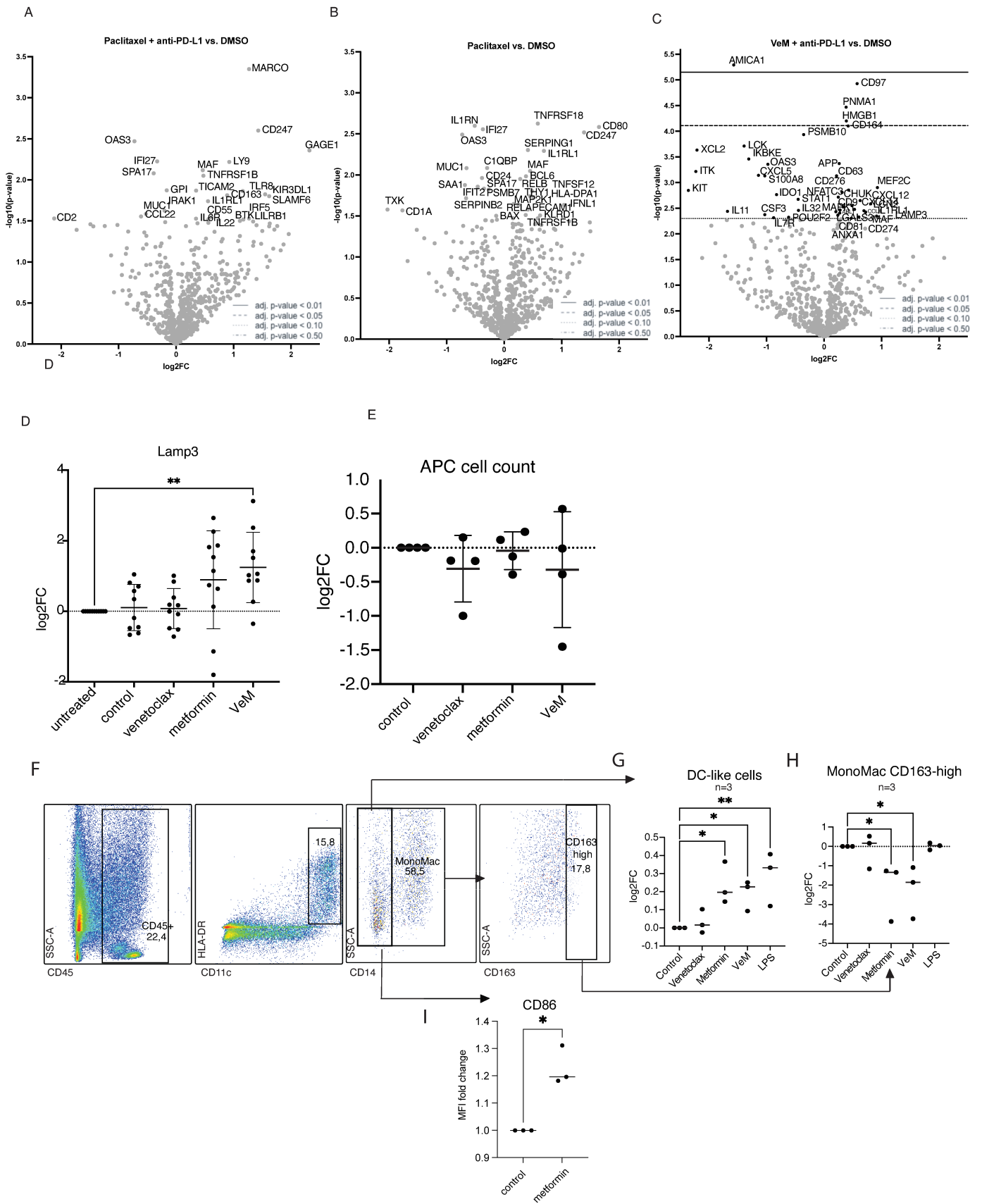
Supplementary Fig 2



Supplementary Fig 3

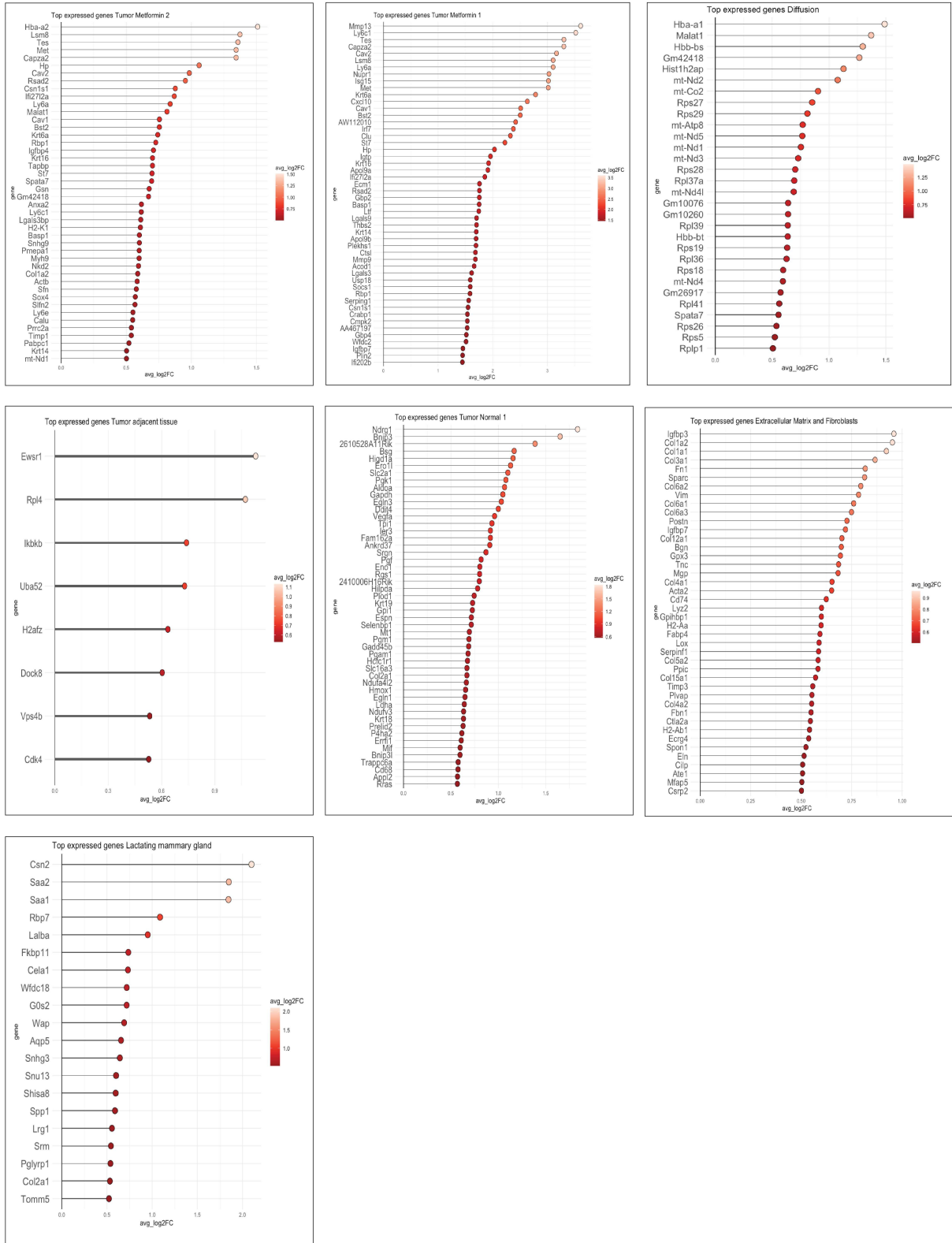


Supplementary Fig 4



Supplementary Fig 6

A



Supplementary Fig 7

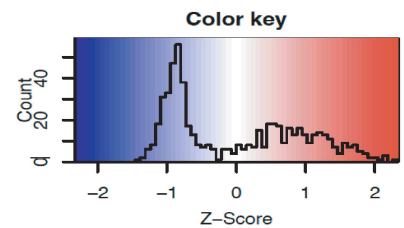
A

metformin vs. control (dendritic cells)

1418.647	918.319	836.901	1118.507	1497.623	763.320	72.770	52.263	98.747	104.481	84.207	79.311
1034.074	616.662	577.521	474.481	1167.315	540.546	84.465	26.132	51.905	48.620	62.586	37.177
533.519	394.201	294.729	198.819	153.919	126.109	2.599	7.317	3.798	3.103	5.690	3.305
875.361	798.190	643.629	564.743	695.445	598.323	291.079	233.094	213.951	184.135	145.655	215.628
253.940	197.545	150.578	119.535	92.127	71.665	7.797	1.045	11.394	3.103	4.552	4.131
1294.118	1313.410	853.887	819.670	936.997	749.987	562.667	575.941	427.902	410.683	464.276	270.981
229.523	193.096	168.941	135.392	141.561	139.998	22.091	41.811	63.299	31.034	21.621	36.351
277.137	212.673	217.144	123.194	212.341	229.441	77.968	49.127	41.777	43.448	46.655	64.441
302.775	288.309	281.874	262.245	261.775	256.107	122.149	116.024	116.470	97.240	93.310	128.055
566.482	497.423	450.815	446.427	552.761	451.659	231.304	214.279	241.803	244.134	238.966	213.150
170.921	106.781	71.157	70.745	48.310	55.555	7.797	1.045	2.532	1.034	0.000	1.652
297.891	280.301	246.066	224.433	252.787	231.663	123.449	118.115	94.949	81.723	73.966	90.052
244.173	168.181	265.807	141.491	216.835	269.440	68.871	75.259	112.672	44.482	69.414	99.139
258.824	217.122	227.244	136.612	155.043	224.441	100.059	67.942	50.639	66.206	63.724	76.007
411.432	391.531	354.409	429.351	332.555	327.772	87.064	83.621	119.002	160.342	136.552	150.361
581.132	473.397	409.039	423.252	458.387	348.327	271.587	226.823	216.483	205.859	188.897	172.668
396.782	347.929	321.814	276.882	311.209	268.329	129.946	131.703	126.598	163.446	117.207	132.186
263.707	282.081	186.386	173.204	155.043	188.330	77.968	83.621	100.013	84.826	62.586	71.050
1097.559	1048.236	734.526	700.134	771.843	838.875	527.581	780.813	341.815	351.718	325.448	390.774
186.793	169.960	115.229	185.401	184.254	146.664	46.781	53.309	43.043	57.930	67.138	36.351
111.099	82.756	113.392	97.580	93.250	83.332	24.690	19.860	25.320	41.379	15.931	29.742
163.596	135.256	122.574	69.526	116.844	97.221	31.187	31.358	22.788	32.068	29.586	26.437
183.130	120.129	123.492	67.086	106.732	82.776	22.091	19.860	11.394	23.793	23.897	10.740
1396.671	1074.932	967.279	925.788	1103.275	923.873	806.965	545.629	600.076	561.715	531.414	521.308
153.829	123.688	135.428	100.019	120.214	119.998	38.984	50.173	50.639	42.413	43.241	39.656
19.534	15.127	30.758	60.987	40.446	26.666	275.486	90.938	281.048	283.444	265.138	166.885
134.295	158.392	153.332	143.930	131.449	167.219	375.544	314.625	320.294	363.098	385.759	361.859
23.196	12.458	26.167	30.494	25.840	12.778	118.251	94.074	106.343	102.412	137.690	93.356
29.301	29.365	31.217	18.296	50.557	48.888	161.133	134.839	149.386	154.135	267.414	223.890
296.670	365.726	219.899	200.038	106.732	71.110	1655.514	1244.911	1622.990	1036.535	724.862	403.993
34.184	49.831	53.253	68.306	44.940	37.777	183.224	122.296	173.440	203.790	130.862	122.272
35.405	34.704	35.349	42.691	20.223	43.333	168.930	116.024	110.141	177.928	93.310	124.750
106.215	106.781	68.862	89.041	117.967	100.554	279.384	232.049	258.261	209.997	281.069	303.201
63.485	62.289	44.531	68.306	46.063	41.666	159.834	151.563	139.258	153.101	117.207	128.055
174.584	141.485	151.496	142.710	150.549	102.221	365.149	232.049	373.465	320.684	357.311	281.721
100.111	88.984	141.396	125.634	93.250	188.886	395.036	220.551	311.432	424.131	355.035	444.475
245.394	268.733	193.731	185.401	144.931	142.220	643.233	745.274	615.268	425.166	398.276	294.113
240.511	290.089	156.087	143.930	125.832	177.219	579.560	593.711	440.562	276.202	419.897	280.895
183.130	243.817	216.226	413.494	311.209	242.774	341.758	372.115	454.488	627.921	594.000	460.998
37.847	54.280	53.712	47.570	69.657	37.777	180.625	142.156	198.759	170.687	232.138	111.532
104.994	161.062	189.600	136.612	132.573	206.108	228.705	332.394	364.603	283.444	358.448	352.771
1132.964	926.328	1047.618	1259.998	1096.534	1024.427	2363.720	1706.918	2369.920	2025.485	2343.001	2042.270
50.056	64.069	18.822	23.175	34.828	20.555	163.732	190.238	127.864	105.516	139.966	68.571
51.276	35.594	59.680	97.580	48.310	97.221	196.219	108.708	156.982	278.271	128.586	199.105
3.663	3.559	8.722	10.978	8.988	2.778	59.775	33.448	81.023	107.584	53.483	19.002
13.430	5.339	14.691	17.076	12.358	12.778	63.674	41.811	64.565	58.965	87.621	56.179
377.248	331.022	348.900	282.981	390.977	386.105	697.811	684.649	640.587	564.818	780.621	636.970
47.614	93.434	84.011	102.459	84.262	83.887	179.326	164.107	243.069	200.686	151.345	166.885
874.140	869.378	811.651	728.189	668.481	654.433	2223.378	1596.120	1455.880	1579.630	1708.035	1452.391
269.811	237.588	326.405	407.395	169.648	217.219	673.121	412.880	600.076	717.919	454.035	369.294

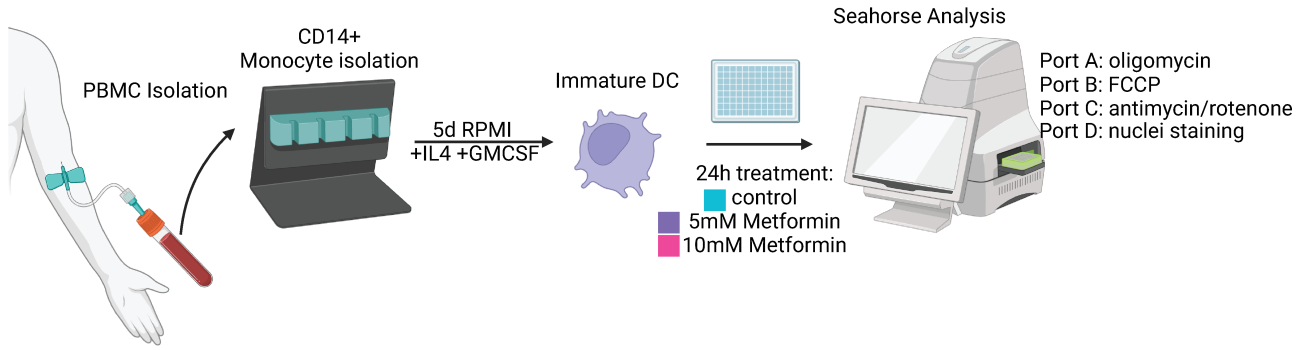
DDIT3 (ENSG00000175197)
TRIB3 (ENSG00000101255)
GDF15 (ENSG00000130513)
ATF4 (ENSG00000128272)
PSAT1 (ENSG00000135069)
GARS1 (ENSG00000106105)
ATF3 (ENSG00000162772)
XPOT (ENSG00000184575)
TARS1 (ENSG00000113407)
CEBPG (ENSG00000153879)
PHGDH (ENSG00000092621)
YARS1 (ENSG00000134684)
SNHG7 (ENSG00000233016)
AARS1 (ENSG00000090861)
MAP3K4 (ENSG00000085511)
SARS1 (ENSG000000031698)
CEBPB (ENSG00000172216)
RIPK2 (ENSG00000104312)
ASAH1 (ENSG00000104763)
RPS6KA2 (ENSG00000071242)
HOTAIRM1 (ENSG00000233429)
SESN2 (ENSG00000285069;ENSG00000130766)
PAG1 (ENSG00000076641)
SLC3A2 (ENSG00000168003)
C15orf61 (ENSG00000189227)
NDRG2 (ENSG00000165795)
DBNL (ENSG00000136279)
WDR54 (ENSG00000005448)
GATM (ENSG00000171766)
MT2A (ENSG00000125148)
RASSF7 (ENSG00000273859;ENSG00000099849)
SIGLEC10 (ENSG00000142512)
FUOM (ENSG00000148803)
LIMD2 (ENSG00000136490)
MIF (ENSG00000267601;ENSG00000240972)
INTS3 (ENSG00000262826;ENSG00000143624)
NCAPH (ENSG00000121152)
UCP2 (ENSG00000175567)
HNRNPM (ENSG00000099783)
HK3 (ENSG00000160883)
SRSF5 (ENSG00000100650)
S100A10 (ENSG00000197747)
MAP1A (ENSG00000166963)
FHOD1 (ENSG00000135723)
LINC02185 (ENSG00000262097)
ALDOC (ENSG00000109107)
BLVRA (ENSG00000106605)
LYST (ENSG00000143669)
ALOX15 (ENSG00000161905)
PFKP (ENSG00000067057)

H_10mM_Met
 I_10mM_Met
 J_10mM_Met
 L_10mM_Met
 M_10mM_Met
 N_10mM_Met
 H_untreated
 I_untreated
 J_untreated
 L_untreated
 M_untreated
 N_untreated

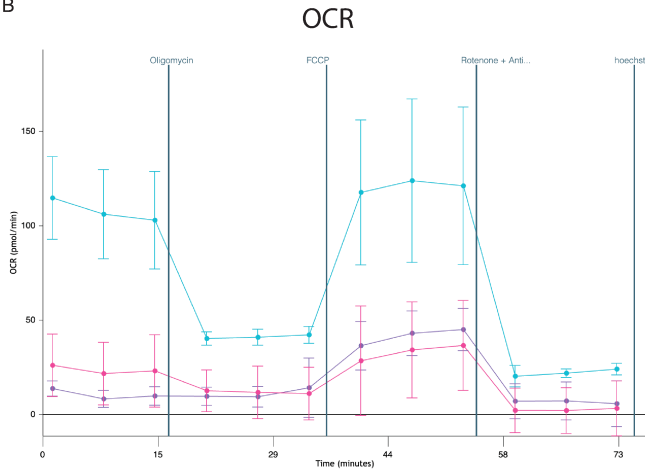


Supplementary Fig 8

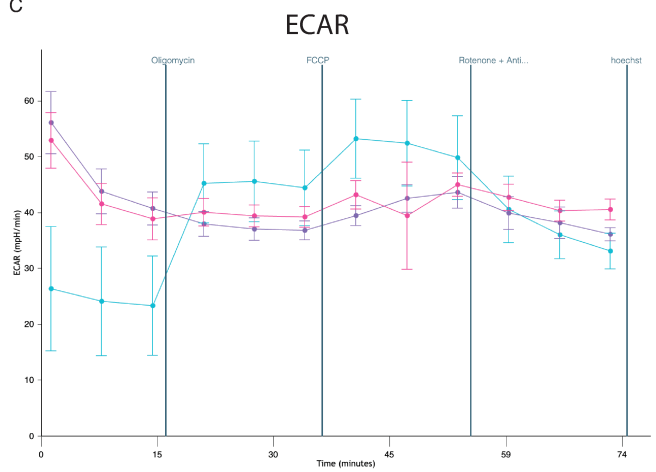
A



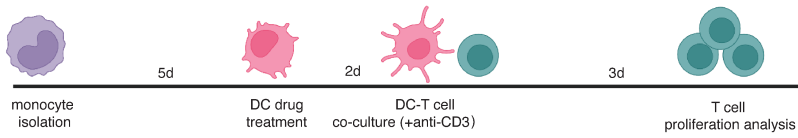
B



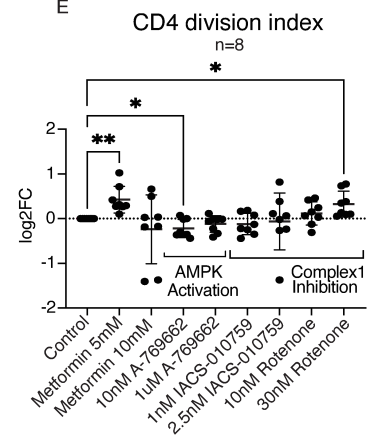
C



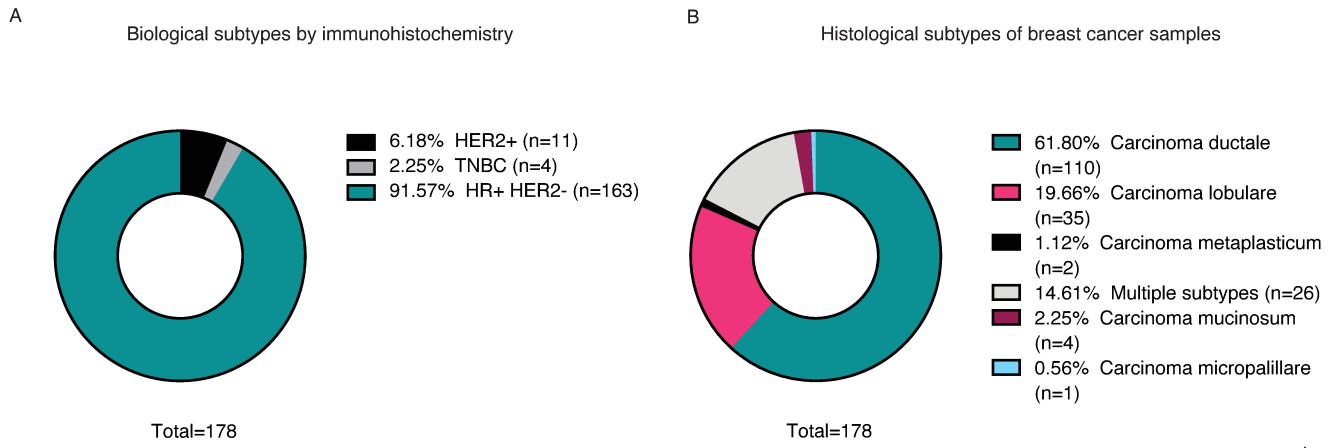
D



E



Supplementary Fig 9



1

Respiratory Complex I Regulates Dendritic Cell Maturation in Explant Model of Human Tumor Immune Microenvironment

Supplementary material

Supplementary Fig. 1. Characterization of PDEC immune clusters and activity pathways **a**, clustering of single cell RNA data into major and **b**, minor immune cell subtypes based on known gene expression profiles for each cell type **c**, volcano plots of the genes used to compare basal activity of pathways including NK cell functions, T cell functions, B cell functions, cytokines and interleukins, TLR, senescence and macrophage functions of PDECs grown 72hrs compared to primary tumor material. The significance of individual genes is separated by horizontal lines of defined adjusted p-values.

Supplementary Fig. 2. Immune cell status of primary tumor material, and flow cytometry analysis of PDECs **a**, Primary tumor immune infiltration of three independent, randomly selected primary breast cancer samples (P832T, P837T, P838T) corresponding to PDECs from figure 2 showing CD45+ leukocytes (yellow) and tumor cells (purple). The scale is 50um. **b-d**, 3-7 technical replicates of fragments within the PDECs of donors P1560T, P1608T, and P1607T. The scale is 10um. Stainings are indicated on the images: Hoechst (blue), CD3 (green), CD45 (red), F-actin (yellow). **e**, flow cytometry gating guide to determine checkpoint marker expression of CD3+ T cells from PDECs. Debris, doublets, and non-viable cells were removed from the analysis. CD45+ leukocytes and CD3+ CD56- T cells were analyzed for figure 2k-o.

Supplementary Fig. 3. MYC protein staining of primary breast cancer tissue **a**, c-MYC staining of 10 biologically independent patient tumors used in Fig 3b. Samples were scored for MYC positivity by from 0-100% in increments of 0-20%, 21-40%, 41-60%, and 61-100%.

Supplementary Fig. 4. Modulation of APCs in response to paclitaxel, VeM, and metformin-alone **a**, volcano plot of gene-expression changes in response to paclitaxel + anti-PD-L1 **b**,

paclitaxel and **c**, Venetoclax +metformin + anti- PD-L1 through nanostring gene expression profiling **d**, RT-qPCR increase of LAMP-3 in 10 PDECs in response to metformin **e**, flow cytometry of absolute number of APCs in 4 PDECs with no significant change in cell numbers **f**, flow cytometry gating used to quantify **g**, the proportion of DC-like cells within the APCs and **h**, the proportion of mono-macs expressing high levels of CD163. Data are presented as mean values +/- SD. Statistical significance was tested with a one-way ANOVA with Fishers exact test. **i**, a statistically significant increase in CD86 expression in DC-like cells following metformin treatment using a student's t-test.

Supplementary Fig. 5. Ex vivo DC characterization and in vivo effects of metformin a, individual datapoints from Fig4e showing the baseline characterization of live CD45+ with varying levels of HLA-DR and CD11c expression **b**, spatial transcriptomics of WapMYC mouse tumor tissue showing decreased CD68 macrophage expression (n=1) following metformin treatment **c,d**, volcano plot of differentially expressed genes in metformin treated tumor tissue

Supplementary Fig 6. Characterization of tissue areas in spatial transcriptomics tumor tissue

a, Top expressed genes used to characterize 9 independent tissue type clusters from spatial transcriptomics data for comparison from WAPMYC mouse tumor tissue

Supplementary Fig 7. Gene expression changes in PBMC-derived DCs following metformin treatment a, 25 upregulated (red) and downregulated (blue) differentially expressed genes of PBMC-derived human DCs in response to 24hr treatment of 10mM metformin from bulk RNA sequencing.

Supplementary Figure 8. Metabolic changes in dendritic cells following metformin treatment, and effects on total T cell division. a, schematic representation of Seahorse extracellular flux assay **b**, OCR values of three donors following control (blue), 5mM (purple) or 10mM (pink) metformin treatment. **c**, ECAR values of three donors following control (blue), 5mM (purple) or 10mM (pink) metformin treatment **d**, schematic of timeline for DC, T cell co-culture assay used in Fig5j-k. **e**, flow cytometry analysis of CD4+ T cell division index

indicating the proportion of the total sample that is dividing (G0-G4) with significant increase in overall CD4+ T cell division following 5mM metformin ($p=0.0050$), and 30nM rotenone ($p=0.0148$) treatments, and a significance decrease in CD4+ T cell proliferation following 10nM A769662 treatment ($p=0.0184$). Statistical significance was tested with a one-way ANOVA with Fishers exact test.

Supplementary Fig. 9. Breast cancer patient molecular and histological subtypes
a, molecular subtypes of patients from which PDECs were derived for this study. HER2+ = ER-, PR-, HER2+; TNBC = ER-, PR-, HER2-, Luminal = ER+, PR +/-, HER2 +/- **b**, histological characterization of patients from which PDECs were obtained for this study.

Supplementary table 1: Flow cytometry antibodies

Target	Color	Species	Target	Clone	Catalog	Company
CD103	unconjugated	Rabbit		EPR22590-27	ab224202	abcam
CD11b	AlexaFluor488	Rat	Human	M1/70	557672	BD
CD11c	FITC		Human	3.9	301604	BioLegend
CD11c	PE	Mouse	Human	3.9	565910	BD
CD11c	unconjugated				PA5-90208	Invitrogen
CD11c	Pe-Cy5	Mouse	Human	3.9	301610	Biolegend
CD123	PE-Cy7	Mouse	Human	7G3	560826	BD
CD123	BV785	Mouse	Human	6H6	2130160	Sony
CD14	BV480	Mouse	Human	MøP9	566141	BD
CD14	BV510	Mouse	Human	MøP9	563079	BD
CD14	APC	Mouse	Human		555399	BD
CD14	Pacific blue	Mouse	Human	M5E2	301828	Biolegend
CD15	PerCP-Cy5.5	Mouse	Human	HI98	560828	BD
CD16	PE	Mouse	Human	B73.1	561313	BD
CD163	BV650	Mouse	Human	GHI/61	563888	BD
CD163	BV786	Mouse	Human	GHI/61	741003	BD
CD163	FITC	Mouse	Human	GHI/61	563697	BD
CD163	BV650	Mouse	Human	GHI/61	563888	BD
CD183	AlexaFluor488	Mouse	Human	1C6/CXCR3	558047	BD
CD184	APC	Mouse	Human	CXCR4	560936	BD
CD19	PE-CF594	Mouse	Human	HIB19	562321	BD
CD19	BV605	Mouse	Human	HIB19	302244	Biolegend

CD1c	PerCP-Cy5.5	Mouse	Human	F10/21A3	565423	BD
CD1c	APC					
CD206	APC-Cy7		Human	15-2	321120	BioLegend
CD206	PE	Mouse	Human		555954	BD
CD3	PerCP-Cy5.5	Mouse	Human	SK7	332771	BD
CD3	Pe-Cy5.5					
CD4	PE-Cy7	Mouse	Human	RPA-T4	560649	BD
CD45	APC-H7	Mouse	Human	2D1	560178	BD
CD45	Pacific orange	Mouse	Human	2D1	PO-160-T100	EXBIO
CD45 (NCL-L-LCA)	unconjugated	Mouse	Human		NCL-L-LCA	Novocastra
CD56	BV421	Mouse	Human	NCAM16.2	562751	BD
CD56	APC-Cy7		Human	HCD56	318332	BioLegend
CD56	APC-Cy7					
CD64	PE		Human	10.1	305008	BioLegend
CD64	PE					
CD66b	AlexaFluor647	Mouse	Human	G10F5	561645	BD
CD69	APC		Human	L78	340560	BD
CD8	BV510	Mouse	Human	SK1	563919	BD
CD80	BV510	Mouse	Human	L307.4	563084	BD
CD80	AlexaFluor647		Human	2D10	305216	BioLegend
CD86	PE-Cy7	Mouse	Human	2331	561128	BD
CD86	PE-Cy7		Human	IT2.2	305422	BioLegend
CD86	Pe-Cy7	Mouse	Human	IT2.2	305422	Biolegend
CD8a	unconjugated	Rabbit		EPR20305	ab209775	abcam
CD8a	Pe-Cy5		Human	HIT8a	300909	BioLegend
EpCAM	PerCP-Cy5.5		Human	EBA-1	347199	BD
Fc epsilon R1 alpha	FITC	Mouse	Human	CRA1	130-117-361	Miltenyi
FOXP3	PE	Mouse	Human	259D/C7	560046	BD
GZMB	PE-Cy7	Mouse	Human	GB11	561142	BD
HLA DR	AlexaFluor 594	Mouse	Human	L243	NB100-77855AF594	Novus Biologicals
HLA-DR	PE		Human	L243	307606	BioLegend
HLA-DR	APC	Mouse	Human		559866	BD
HLA-DR	APC-R700	Mouse	Human	G46-6	565127	BD
LAG-3	PE		Human	3DS223H	12-2239-42	eBioscience
Mannose Receptor	AlexaFluor 700	Mouse	Human	15 2	321132	Biolegend
PD1	FITC	Mouse	Human	MIH4	557860	BD
PDL1	PE-Cy7	Mouse	Human	MIH1	558017	BD

PDL1	PerCP-Cy5.5	Rat	Human	MIH5	NBP1-43262PECY55	NovusBio
Propidium Iodide					421301	Biologend
PDL2 (CD273)	APC	Mouse	Human	MIH18	557926	BD
CD45	BV421	Mouse	Human	L161	331541	Biologend
CD11c	FITC	Mouse	Human	3.9	565910	Biologend
HLA-DR	PE	Mouse	Human	L243	307606	Biologend
CD14	BV510	Mouse	Human	MφP9	563079	BD
CD86	PE-Cy7	Mouse	Human	IT2.2	305422	Biologend
CD83	PerCP-Cy5.5	Mouse	Human	HB15e	305320	Biologend
CD40	APC	Rat	Human	3/23	124611	Biologend
CD1a	BV711	Mouse	Human	HI149	300139	Biologend
CD1c	BV650	Mouse	Human	L161	331541	Biologend

Supplementary table 2: IHC antibodies

Target	Fluorochrome	Species	Target	Dilution	Catalog	Company
FoxP3	TSA-488	Mouse	Human	1:200	ab20034	Abcam
CD3	TSA-555	Rabbit	Human	1:750	MA5-14482	Invitrogen
CD8	Alexa-647	Mouse	Human	1:300	M7103	DAKO
CD4	Alexa-750	Rabbit	Human	1:25	ab133616	Abcam
CD45	Alexa-647	Rabbit	Human	1:100	CST13917	Cell signaling technology
PanEpi Cocktail (PanCK, E-cadherin)	Alexa-750	Mouse	Human	1:150 1:100 1:200	ab7753, MA5-13156, 610182	Abcam Invitrogen BD
CD8a	Unconjugated	Rabbit	Mouse	1:2000	ab209775	Abcam
CD103	Unconjugated	Rabbit	Human/ Mouse	1:5000	ab224202	Abcam
c-MYC	Unconjugated	Rabbit	Human/ Mouse	1:200	ab32072	Abcam

Supplementary table 3: Primers

Name	Primer nucleotide sequence (5'-3'):
Human Arg1 Forward	GAAAGGCTGGTCTGCTTGAG
Human Arg1 Reverse	CACAGACCTTGGATTCTTCACA
Human iNOS Forward	AATCTCTGGTCAAGCTGGATG
Human iNOS Reverse	GCAAGATTTGGACCTGCAAG
Human Lamp3 Forward	TTGACCGTCTCAGATCCAGA
Human Lamp3 Reverse	CTCTGTTCACCTCACGCACTT
Human CIITA Forward	TACTCAGAACCCGACACAGA
Human CIITA Reverse	CCGATCACTTCATCTGGTCC
Human IFNy Forward	TTAATGCAGGTCATTTCAGATG
Human IFNy Reverse	AGACAATTTGGCTCTGCATT
Human CD47 Forward	TAGATCCGGTGGTATGGATG

Human CD47 Reverse	ATATTCACCTGGGACGAAAG
Human PRF1 Forward	CGCCTACCTCAGGCTTATCTC
Human PRF1 Reverse	CCTCGACAGTCAGGCAGTC
Human GZMB Forward	CCCTGGGAAAACACTCACACA
Human GZMB Reverse	CACAACTCAATGGTACTGTCGT
Human GAPDH Forward	CTCTGCTCCTCCTGTTTCGAC
Human GAPDH Reverse	GCCCAATACGACCAAATCC
Human ActB Forward	CTTACCACCACGGC
Human ActB Reverse	CCATCTCTTGCTCGAAG
Human PUM1 Forward	GCCCCAGTCTTTGCAATTA
Human PUM1 Reverse	AATCACTCGGCAGCCATAAG